sustainability

MDPI

Article

Minimally Invasive Retrofitting of RC Joints with Externally Applied SMA Plate—Adaptive Design Optimisation through Probabilistic Damage Simulation

Mohammad Amin Molod [1,2], Franz-Joseph Barthold [1] and Panagiotis Spyridis [1,*]

[1] Faculty of Architecture and Civil Engineering, TU Dortmund University, 44227 Dortmund, Germany
[2] Department of Civil Engineering, Faculty of Engineering, Soran University, Diana 44008, Iraq
* Correspondence: panagiotis.spyridis@tu-dortmund.de

Abstract: Beam–column joints are the critical section of many reinforced concrete (RC) structure types in which any failure could lead to the collapse of the entire structure. This paper attempts to employ a superelastic shape memory alloy plate as an innovative and adaptive external strengthening element to rehabilitate existing concrete beam–column joints and enhance the structure's performance. An experimentally investigated beam–column joint is used as the case study, and it is investigated numerically to validate the effects of an innovative strengthening technique based on shape memory alloys. The results show that the proposed technique could increase the joint's stiffness and reduce the risk of overall failure. A particular innovation in the proposed method is associated with the novel material itself but also with the fact that the increased potential costs of using special alloys are counteracted by its potential to produce these elements in an optimised industrially produced fastened plate. This fits-all construction product further allows a rapid and minimally invasive strengthening technique. Moreover, to achieve this, the plate is adaptively designed against random critical load combinations through probabilistic damage prediction.

Keywords: shape memory alloy; reinforced concrete; beam–column joints; probabilistic damage analysis; non-linear finite elements; ansys APDL; MATLAB

Citation: Molod, M.A.; Barthold, F.-J.; Spyridis, P. Minimally Invasive Retrofitting of RC Joints with Externally Applied SMA Plate—Adaptive Design Optimisation through Probabilistic Damage Simulation. *Sustainability* **2023**, *15*, 3831. https://doi.org/10.3390/su15043831

Academic Editor: Jorge de Brito

Received: 10 January 2023
Revised: 15 February 2023
Accepted: 16 February 2023
Published: 20 February 2023

1. Introduction

1.1. Motivation, Fundamental Principles, and Background Knowledge

This article is written just days after a catastrophic series of earthquakes hit densely populated areas in southern and central Turkey, as well as northern and western Syria, in early February 2023 [1]. The extent of the damage is still being assessed, but the disaster is already recognized as one of the most severe in recent history [2,3]. Its impacts are magnified by the coincidence of encumbered public welfare provisions in the region due to military hostilities, the pandemic, financial distress and very low temperatures in the region. This again brings to the forefront the enormous significance of the protection of the existing building stock, be that from earthquake events or extreme climate change-induced natural hazards in general. Moreover, structural interventions need to have enhanced characteristics such as being rapid, minimally invasive, cost-effective and subsequently financially viable, in order to qualify as adequately resilient solutions. Some examples with various novel materials and techniques can be found in [4–9], and a state-of-the-art report and guidance in [10]. The research reported below seeks to address this issue with a focus on the use of advanced superelastic shape memory alloys for use at the critical joint locations of framed concrete structures.

Concrete has been one of the most commonly used construction materials for decades. Despite its high and reliable compressive strength, its brittle nature and low resistance under tensile loads cause cracking at the initial service life of the structure. Concrete cracking can impede its mechanical and structural properties, such as stiffness, strength, service

life, resilience and durability [11]. Propagation and growing crack width can lead the steel reinforcement to be exposed to the environment and subsequently oxidised, reducing the cross-section area of the bars. Hence, their capability and resistance as tension members will deteriorate, potentially resulting in complete structural failure. Abdulrahman et al. [12] and Shanmugam et al. [13] have conducted numerous investigations on this topic. Beam–column joints are the most critical locations of concrete structures whose failure can lead to the collapse of the entire structural system. This beam–column performance and its crucial role in overall structural safety (particularly under lateral seismic loads) is discussed in detail in [14,15]. Damage propagation in a framed system entails significant uncertainties—due to, e.g., the seismic excitation but also the distribution of strength and stiffness in beams and columns—and, therefore, robustness criteria need to be applied by assigning adequate capacity in selected elements of the structure [16]. Robustness design with consideration of such uncertainties (see [17–19]) is the state-of-art approach in modern structural engineering. This situation renders joint strengthening before damage or rehabilitation after partial damage essential. Structural repair has increased unprecedentedly worldwide, and its annual maintenance outlay is higher than that of new construction [19–21]. Rehabilitation can be achieved via a an additionally applied strengthening element; existing technologies in the literature include primarily special concrete layers [22–25], metal-confining assemblages [26,27] or fibre-reinforced polymers (FRP) [28–32].

Superelastic shape memory alloys (SMA), i.e., alloys with significant deformation reversal potential, can be an ideal option since they offer a spectrum of structural material properties [33] that can suitably increase the strength and resilience of joints. Investigations on the employment of SMA as a strengthening element of concrete members have hence been intensified in the last years [34–38]. A comprehensive overview of the application of SMA in civil infrastructures, including steel, concrete, and timber structures, is offered by Zareie et al. [39], for strengthening and repair applications for concrete structures in [40], and in a review from the perspective of multifunctional properties of the alloy by Abavisani et al. [41]. Moreover, SMA are employed in both steel and concrete beam–column joints. Leon et al. [42] describe SMA tendons in the connection section of steel beam–column joints as the main element to transfer loads. The superelastic effect of the alloy was also employed for seismic performance applications in steel structures, for example, by Wang et al. [43] in the form of bolts and by Fang et al. [44] as Belleville washers to enhance the ductility of joints. SMA bolts are reported in [45] to enable an improvement in the initial stiffness, shear resistance and energy dissipation capability of steel beam–column joints. Regarding concrete structures, Molod et al. [46] provide a comprehensive literature review of SMA applications. Varela [47] presents nickel-titanium (NiTi) SMA bars as a connection tool to link reinforced concrete (RC) columns to the concrete footing. The results showed that the proposed concept worked well without considerably damaging the column components under applied ground motion. Wang and Zhu [48] examined the influence of NiTi superelastic SMA as reinforcement in the plastic hinge region of RC shear walls. It led to less energy dissipation, no residual deformation upon unloading, and a significant enhancement in ductility that allowed the wall to tolerate a greater load causing larger displacement. Sensitivities on reinforcement arrangement including hybrid FRP/SMA systems for shear wall bases under different approximation methods are demonstrated in [49]. As shown by Michels et al. [50], an RC beam with externally bonded Fe-SMA strip using direct fixings under static loading showed a higher cracking and ultimate load, as well as ductility, compared to unreinforced and carbon FRP (CFRP)-reinforced beams. Jung et al. [51] showed a reduced residual inter-story drift ratio of a concrete frame by embedding a composite of SMA wires glued together using epoxy resin and covered by a layer of FRP in the plastic hinge region of beam–column joints. Mas et al. [52] used NiTi-SMA cables as longitudinal reinforcement in the tension zone of the concrete beam, indicating considerable robustness and durability. An innovative prestressing application for flexural strengthening, in particular by fastened strips, based

on experimental and analytical studies is presented by Strieder et al. in [53]. A broad palette of strengthening concepts is found in the cumulative work of Schranz [54]. Suhail et al. [55] proposed the use of cables with a shape memory effect to tie pre-damaged concrete beam–column joints loaded under a cyclic loading action. An experimental and numerical investigation on concrete beam–column joint retrofitting is demonstrated by Yurdakul et al. [56], in which NiTi SMA bars were installed diagonally through the joint. This led to a tolerable post-damage condition even under an 8% drift ratio. Elbahy et al. have experimentally [57] and numerically [58] employed superelastic SMA bars to strengthen concrete beam-column joints under a ground motion load, in which the bars were attached parallel to the beam using external rigid steel angles and bolts. The method tolerated higher earthquake intensities and decreased the maximum and residual drifts. Embedding a hybrid NiTi superelastic SMA and glass FRP (GFRP) component in the plastic hinge region of a concrete beam-column joint performed by Youssef et al. [59] indicates a reduced failure load and displacement under pushover analysis. Youssef et al. [60] also tested NiTi SMA bars within the plastic hinge region linked to steel bars on either side using a mechanical coupler. Under cyclic action, the SMA bars in the plastic hinge region showed a larger deformation capability and negligible residual strain. Better performance by the concrete beam-column joint reinforced with the SMA bar under a seismic load in terms of energy dissipation and residual displacements has also been reported in a numerical investigation by Alam et al. [61]. Hojatirad and Naderpour [62] have numerically studied the influence of embedded NiTi SMA bars in concrete frames under 13 far-field earthquake records. The results reported a significant increase in their ductility, maximum drift, and resistance to collapse. In another numerical investigation by Nahar et al. [63], the influence of SMA bars embedded within concrete beam-column joints under pushover analysis on maximum and residual drift and seismic vulnerability was studied. In [64], the employment of superelastic SMA bars within seismically loaded RC beam-column joints reduced inter-storey drifts. Zafar and Andrawes [65] were able to improve the structural performance of an RC frame under a suite of ground motion records in a numerical investigation with an embedded composite of superelastic SMA and FRP.

1.2. Novelty and Significance of this Study

The main aim of this research is to use SMA in a plate format as an externally strengthening element of concrete beam–column joints. As discussed above, SMA have been used in different forms of bar, cable and composite to strengthen the structures. However, the influence of a plate format, specifically to enhance concrete beam–column joints, has not yet been investigated. The innovation in the proposed method is associated with the use of this novel material itself, but also with the proposition that the increased potential costs of using SMA are counterbalanced by supplying strengthening components as an optimised fastened plate through industrialised off-site production. Towards this objective, the plate is adaptively designed against a realistic range of critical load combinations based on "probabilistic damage simulation". This is also a novel methodology, one that creates a reference for designing a strengthening component for a structure accounting for multiple possible damage situations. The newly introduced technique and design concept offer a new paradigm in delivering structurally efficient but also sustainable and resilient strengthening solutions.

1.3. Overview of the Paper Content

Following the introduction above, which intends to put the study in the perspective of modern societal needs for retrofitting schemes but also provides a relevant state-of-practice to highlight its differentiations and novelty, the following main sections are delivered. Section 2 gives a short historical development perspective and the main technical properties of the shape memory alloy materials used. Section 3 provides a thorough description of the methodology followed, including the creation and validation of the basic finite element model. This section further provides the various analysis and computational techniques

employed to dimension and evaluate the attached shape memory alloy-based strengthening component. Representative results are described and discussed comparatively in Section 4. The thought-process and recommendations of the general design approach for such an intervention are given in Section 5, which is followed by a summary with the main conclusions and take-aways in Section 6. A list of nearly 100 technical references is provided at the end. Further insights into the study may be found in the relevant dissertation by Molod at the Technical University of Dortmund [66]. Additional information on the finite element model formulations and input properties, a table of symbols and notations, as well as a flowchart of the prepared algorithms can be found in the "Supplementary Materials" file.

2. Brief Outline of SMA

The history of SMA goes back to 1932, when Chang and Read [67] first recorded SMA transformation properties in a gold–cadmium alloy. Its use was later established in high-end sectors such as aerospace engineering and the robotic and automotive industries. Among all types of SMA, NiTi alloys have found most use in civil engineering [68]. SMA may possess two crystal forms, i.e., Austenite and Martensite. In addition, there are two Martensite transformations: (a) the shape memory effect (see Figure 1), which results from a temperature-induced shift, and (b) shape memory elasticity (see Figure 2), which is caused by external stress-induced transformation.

The main features that distinguish SMA from conventional steel bars are their higher recoverable elongation, higher tensile strength and better corrosion resistance. Table 1 presents a comparison between the properties of SMA and standard reinforcement steel.

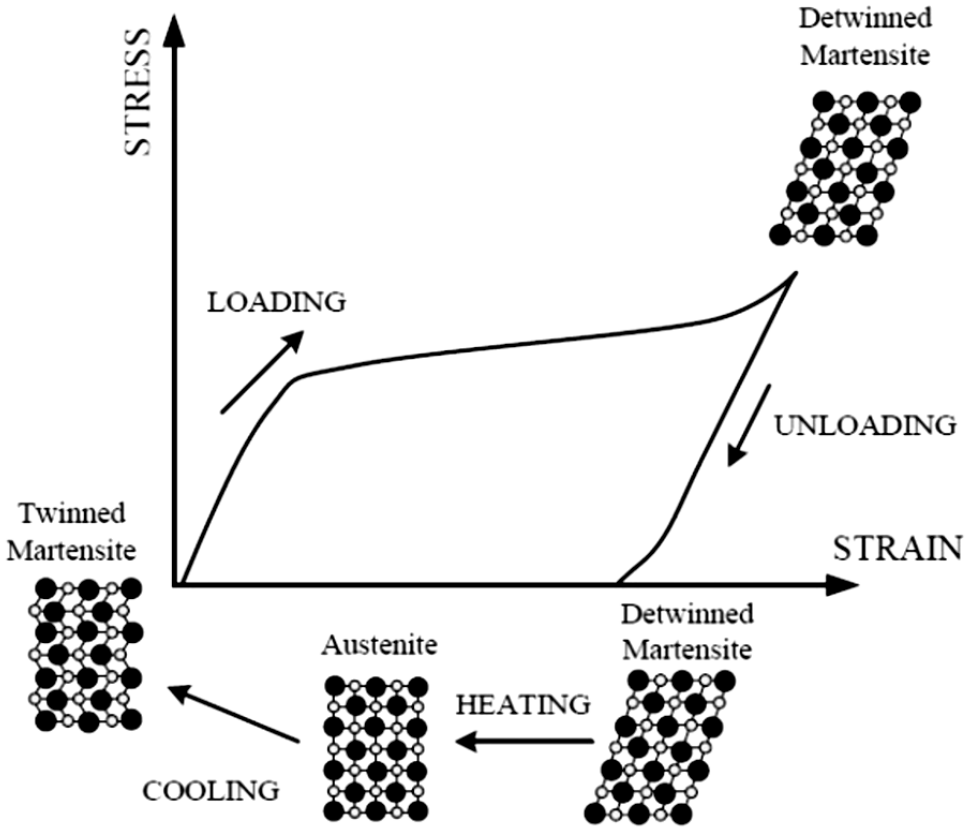

Figure 1. Shape memory effect form [31].

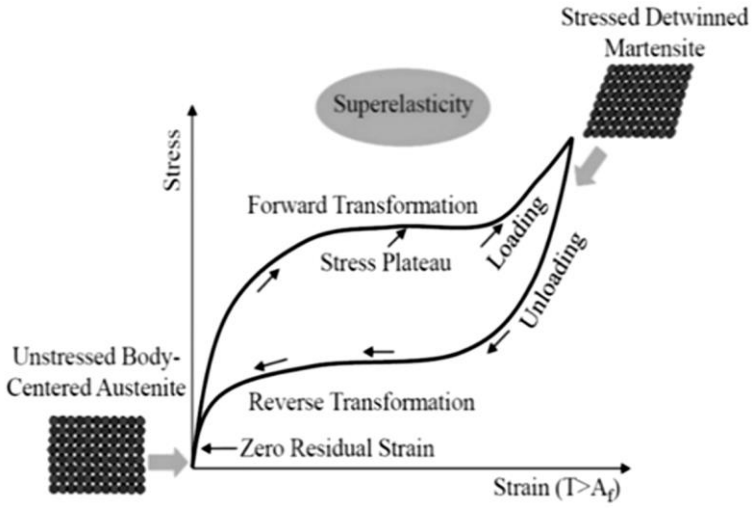

Figure 2. Superelastic shape memory alloy form [32].

Table 1. Indicative comparison of properties of NiTi SMA versus steel [69,70].

Properties	NiTi Alloy (Nitinol)	Standard Steel Rebar
Recoverable elongation	8%	0.2%
Young's Modulus	83×10^3 MPa Austenite $28–41 \times 10^3$ MPa Martensite	2.07×10^5 MPa
Yield Strength	195–690 MPa Austenite 70–140 MPa Martensite	248–517 MPa
Ultimate Tensile Strength	Fully Annealed 895 MPa Work Hardened 1900 MPa	448–827 MPa
Elongation at failure	248–517 MPa	20%
Corrosion Resistance	Excellent	Fair
Cost	Expensive	Fair

3. Description of Research Methodology

3.1. Model Set-Up

3.1.1. Model Overview

A concrete beam–column joint can be located in different parts of a structure, such as the very top corner or middle of a frame. It can have different dimensions and respond to various loading conditions. To address these considerations, the available data of an experimentally investigated joint with a predefined rescaled size under a specific load combination are considered as the case study. This consideration allows the author to check the validation and verification of the numerical results. The joint is simulated in the finite element analysis software Ansys APDL [71]. Figure 3 shows details of the reinforcement and the geometry of the joint. Since it is symmetric, only half of the beam–column joint is modelled to reduce computational time.

Initially, an investigation was conducted to select suitable elements for this research to model concrete and steel rebar in Ansys. Solid element 65 with a hexahedral shape was utilised to model the concrete material. Solid element 185 was used to simulate the SMA plate. The hexahedral form of the element was applied in the probabilistic analysis step, but it was then switched to a tetrahedron due to the meshing complexity of the plate geometry after the optimisation step. To simulate conventional steel bars, the element of Reinf264 was employed. The prior creation of base solid element nodes was required to generate the element. In addition, elastic bearings were simulated at the load application point and the support boundary conditions using the element 45, which accommodates stress peaks and distortions in concrete. Three bearings were created for exerting loads on the system: (i) axial column load, (ii) bending load, and (iii) shear force. Five others were also created for boundary conditions, including four to avoid movement in the X-direction: two at the

top-left and top-right sides of the upper column and two others at the bottom-left and bottom-right sides of the lower column. Another one was placed at the bottom of the lower column to avoid the movement of the system in the Y-direction.

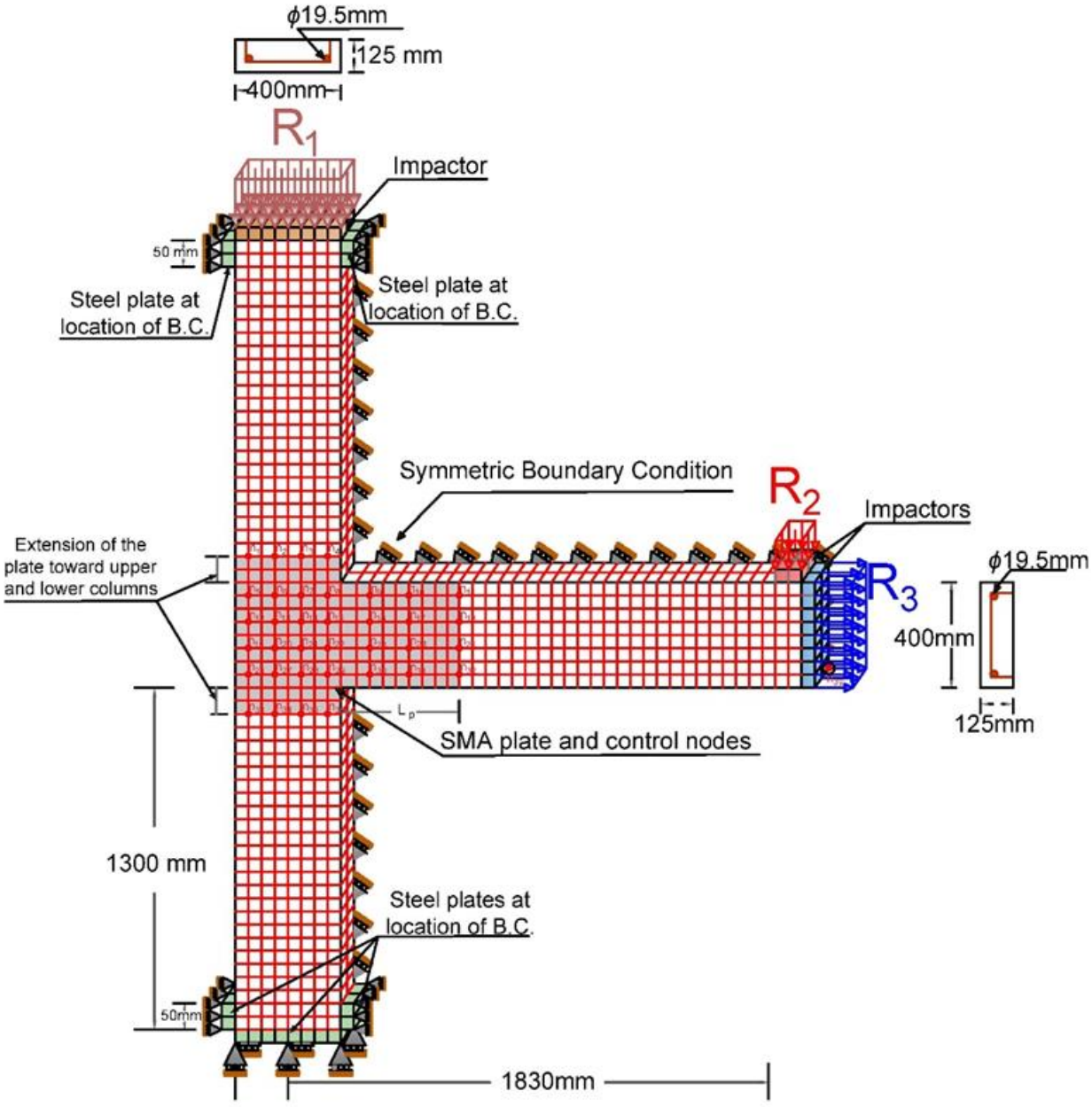

Figure 3. Details of concrete beam–column joint simulated in Ansys.

Furthermore, the symmetric boundary condition was applied to the system, in which movement of those nodes located at the half depth of the system (Z = 125 mm) was closed in the Z-direction. The Young's modulus of the concrete material was not given in the experimental investigation, and it was estimated using current design standards [72] based on the given compressive strength of the concrete. The Poisson's ratio of the concrete was assumed to be 0.2. The uniaxial tensile and compressive strength values were taken equal to 3.5 and 53.5 MPa, respectively, from the experimental investigation. Shear transfer coefficients for an open and closed crack were set to 0.3 and 0.7, respectively. The stiffness multiplier for a crack in tension regions was set to 0.6, and the rest of the material constants were kept as default. A multilinear isotropic hardening model was employed to simulate the non-linear behaviour of the concrete. The main reinforcement of the column and the

beam had the same properties: Young's modulus was 193 GPa, Poisson's ratio was 0.3, and the yielding and ultimate stresses were set to 520 and 630 MPa, respectively. The shear reinforcement had the same Young's modulus and Poisson's ratio as the longitudinal bars, but its yielding and ultimate stresses were 422 and 682 MPa, respectively. The tangent modulus was assumed based on the steel grade and data reported by Shukri and Jumaat [73]. The elongation of the bars was found to be 18 mm; accordingly, the tangent modulus was calculated to be 620.16 MPa and 1461.75 MPa for the main reinforcement and stirrups, respectively. Figure 4 illustrates all input data and assumptions to model SMA in Ansys.

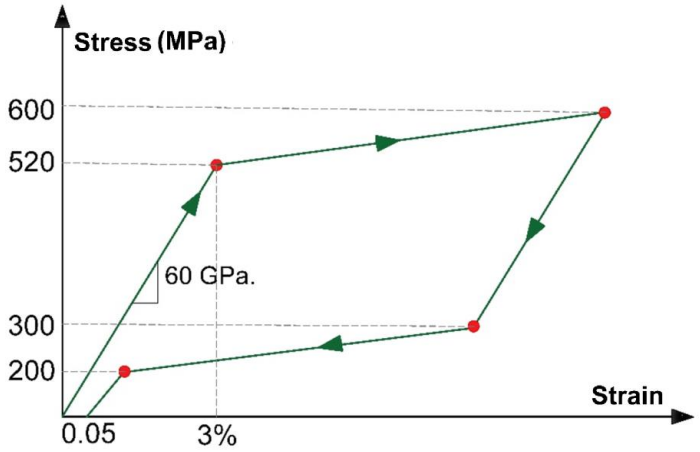

Figure 4. Input data and material model used to simulate SMA in Ansys.

3.1.2. Model Validation, Element and Material Selection

An experiment by Youssef et al. [60] was chosen for this study since all required inputs were available and numerical results could be validated to ensure whether the simulated model was representative. The experiment was conducted at the University of Western Ontario. The concrete beam–column joint was taken from the sixth floor of an eight-storey building designed per the Canadian standards CSA A23.3-0.4 [74] and scaled down to 3/4 of its original size. Furthermore, applied loads were scaled down with a factor of $(3/4)^2$, i.e., the axial column force of 620 kN. It was scaled down to 350 kN, and the reinforcement included four bars with a diameter of 19.5 mm as principal reinforcement and stirrups with an 11.3 mm diameter at an 80 mm spacing in the joint region; the same rebar layout was used for the beam.

There are numerous elements and material models defined in Ansys to simulate RC. Nine combinations of elements and material models were considered and tested against their validation of the experimental data. To model the material concrete, three different material models, respectively using the elements CPT215 and solid65, were employed. The first two material models were based on the microplane model, which simulates the behaviour of the material by stress–strain laws for individual planes and is considered well-suited for cement-bound aggregates of varying properties [71,75,76]. There were two model types: (i) an elastic microplane model with damage and (ii) a coupled damage plasticity microplane model. The constitutive laws of both microplane models are shown in Figures 5 and 6. Both models were based on research done by Zreid and Kaliske [77–80]. Implementation in Ansys used the CPT215 solid element with eight nodes and the capability of stress stiffening, large deflection, elasticity and large strains. The third model was the Menetrey–Willam constitutive model developed by Menetrey [81], extending from the Willam–Warnke yield surface model (see Figure 7) introduced by Willam [82], modelled with the solid element 65. This is a 3D element with eight nodes capable of cracking under tension in three orthogonal directions, crushing under compression, plastic deformation and creep. There are also numerous elements available in Ansys to model steel reinforcements; three quite common elements, namely Reinf264, Link180 and Beam188,

were employed. Unlike Link180 and Beam188, an underlying node structure of solid elements is a prerequisite for the generation of Reinf264. All three elements support bilinear isotropic hardening (see Figure 8).

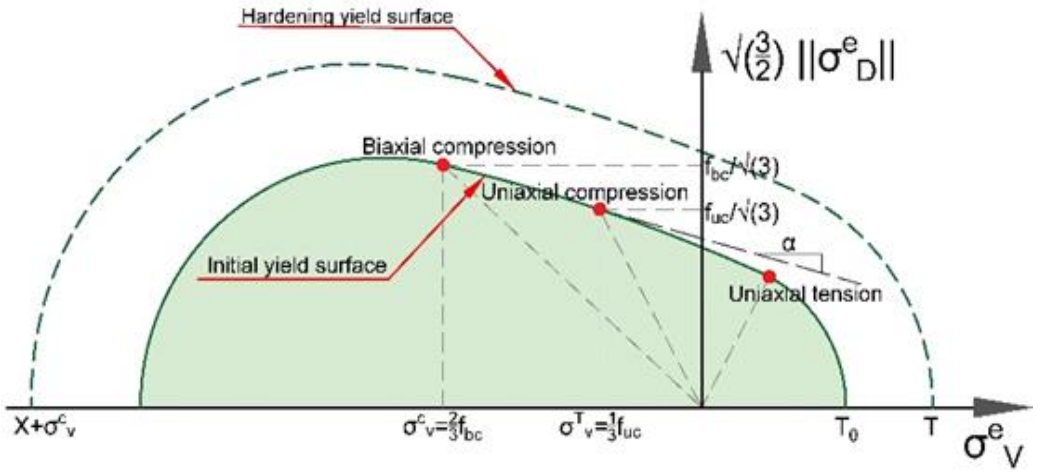

Figure 5. Coupled damage–plasticity microplane model.

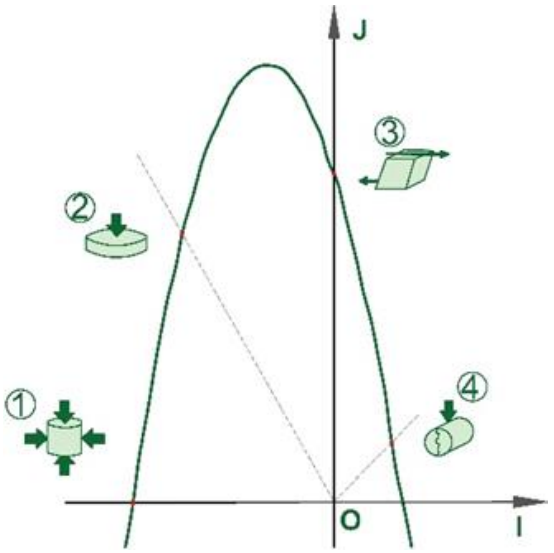

Figure 6. Elastic microplane material model.

An axial column load equal to 350 kN and a bending moment load under displacement control up to 73 mm at the beam's free end were applied. The "WebPlotDigitalizer" software application developed by Rohatgi [83] was utilised to identify the exact data of the graph. Graphs of all models were in good agreement with the experiment in the elastic regime. Nonetheless, in the plastic regime, most cases overestimated the experimental response, indicating that the element types are significant for the damaged system's behaviour. The behaviour of models with Reinf264 was closer to the experiment (see Figure 9). By juxtaposing the load–displacement curves of the models and the experiment, the element combination Solid65 and Reinf64 qualified as the most compatible in terms of load–displacement behaviour, with yielding load and displacement being 58 kN and 15 mm, respectively. This combination was used for further investigations.

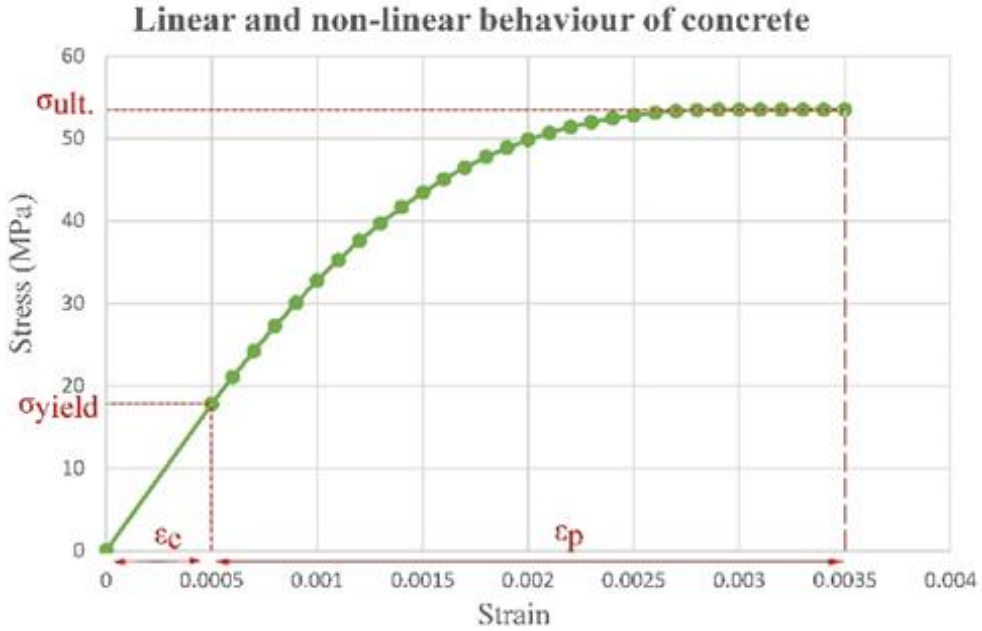

Figure 7. Concrete behaviour defined for Solid 65.

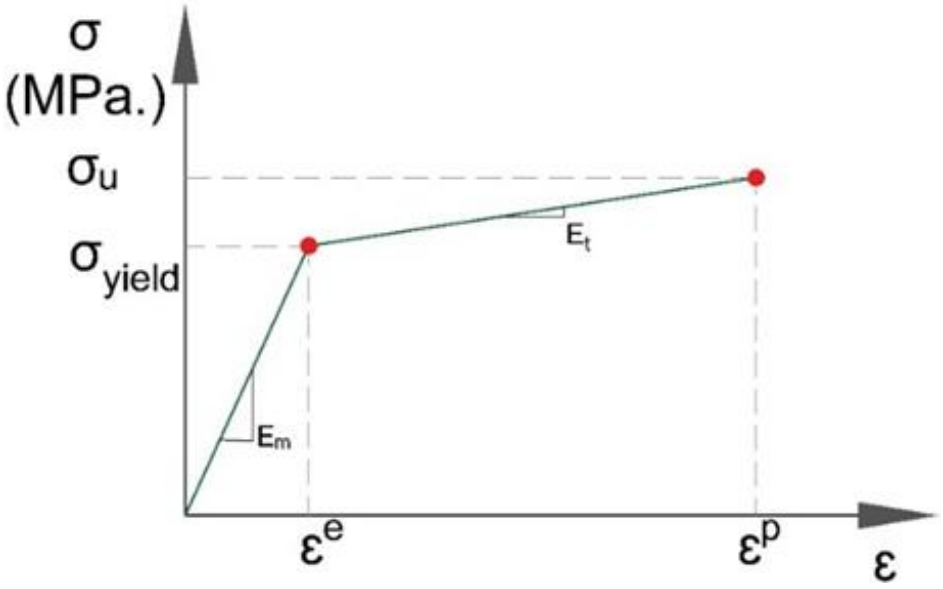

Figure 8. Bilinear isotropic hardening material model of steel rebar.

A mesh size convergence study with a structured mesh system was carried out with ten different element sizes to determine the most appropriate element size. Maximum displacement versus the number of elements was plotted in a diagram. The correct mesh size was achieved once the results of two consequences run with different element sizes remained equivalent. The element size was set to 25 mm. The system was then subjected to specific loading combinations, and the reaction forces computed by the software were compared to hand calculations to verify numerical results.

More information on the elements and materials used as well as the model validation can be found in the "Supplementary Materials" file.

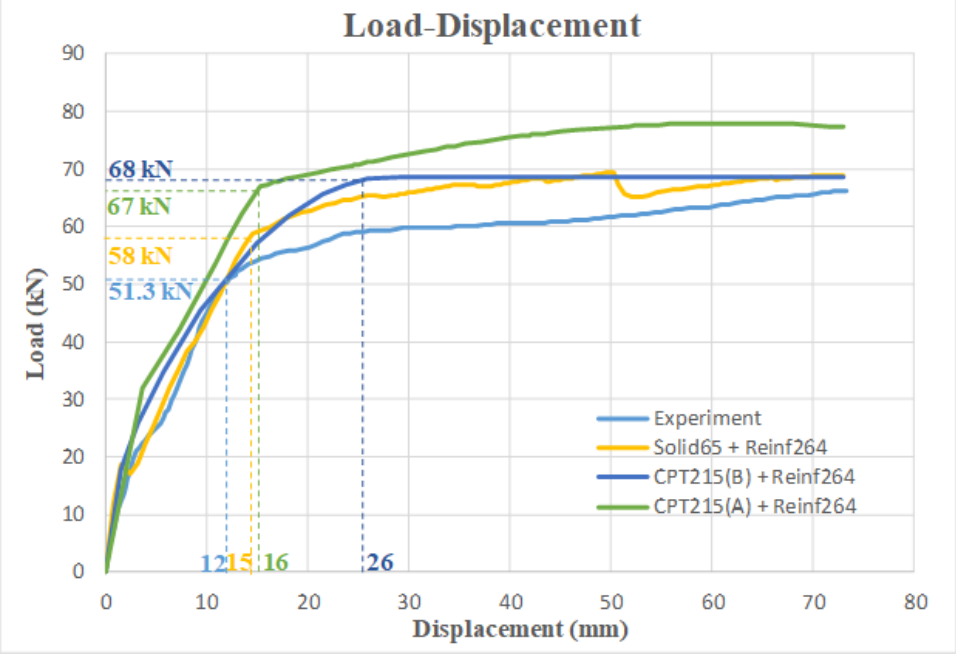

Figure 9. Load–displacement curves of the models in comparison to the experiment.

3.2. Load Combinations' Selection and Designation Initial Geometry of the SMA Plate

Three loads, namely R_1, R_2 and R_3, were applied to the system. R_3 is used only for the stability of the system. The relationship between the loads was calculated and plotted in Figure 10. As shown, the association between possible loads produced a volume of acceptable combinations within the failure safety margin. The external surfaces of this volume, which represented all possible design points, were considered the boundary of the ultimate limit state. Then, this surface was finely triangulated, which generated a large number of nodes located on the limit state surfaces. Each node was defined by three coordinates (x, y and z) representing a failure combination of R_1, R_2 and R_3. These coordinates were conveyed into a self-programmed MATLAB algorithm, and one thousand thereof were randomly selected and individually applied as loading conditions. After the structural analysis was carried out, the steel bars' maximum free-end displacement and maximum axial stress were extracted. The process used a do-while loop for all 1000 simulations, and the results were recorded in one single output file. After completing the loops and scanning for maxima through the output file, the critical load combination was found. The critical load combination corresponded to an axial column force of 2100.20 kN, a bending moment force of 82.77 kN, and zero axial beam force, leading to a maximum displacement of 26.25 mm at the free end of the beam and a maximum stress of the steel bars of 522.5 MPa. This exceeded the yielding stress of 520 MPa and led to the failure of the system. Figures 11 and 12 demonstrate the displacement distribution of the system and axial stress of the steel bars under the critical load combination.

This procedure also allows for a "probabilistic damage simulation" which is used as a spectrum of reference situations as a basis for the design of a strengthening component that can serve multiple possible damage scenarios. This methodology was developed in the context of this study, but it conceptually relies on previously established concepts for the stochastic simulation of existing structures' degradation based on advanced computing methods and on inverse damage identification with the stochastic elaboration of uncertainties and non-linear finite element modelling (see also [84–87]).

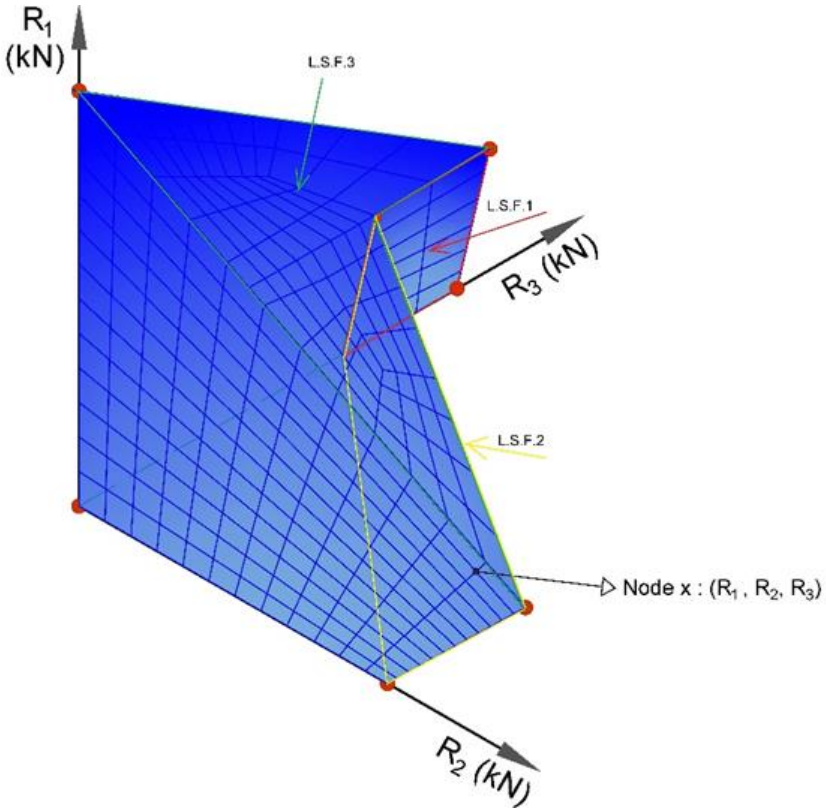

Figure 10. Schematic view of relationships between loads R_1, R_2 and R_3.

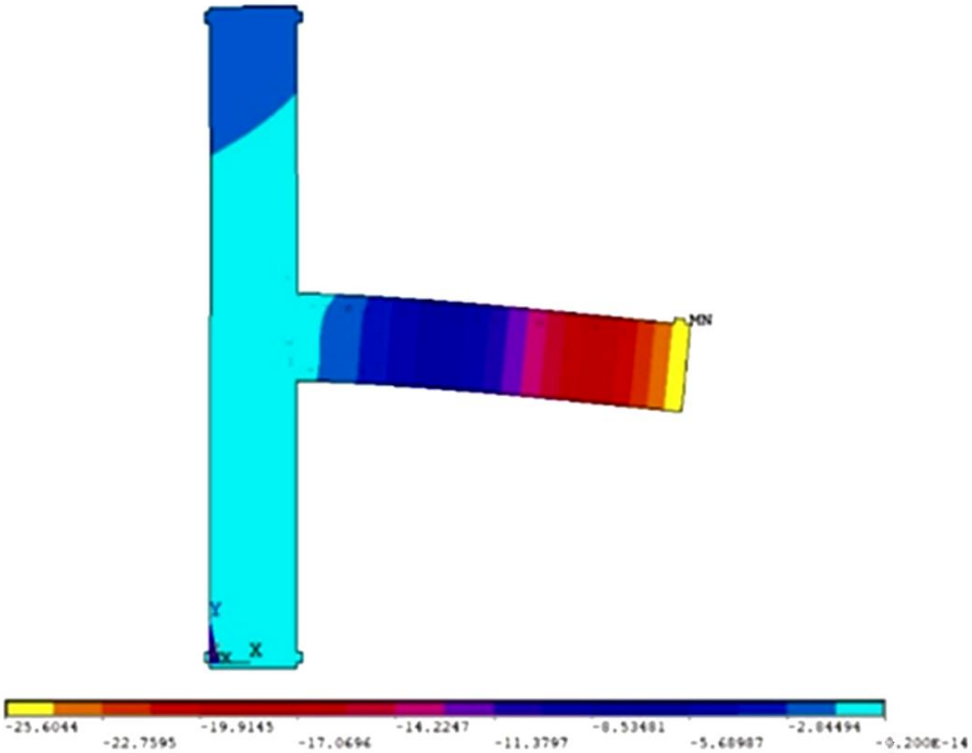

Figure 11. Maximum displacement and related deformation spectrum.

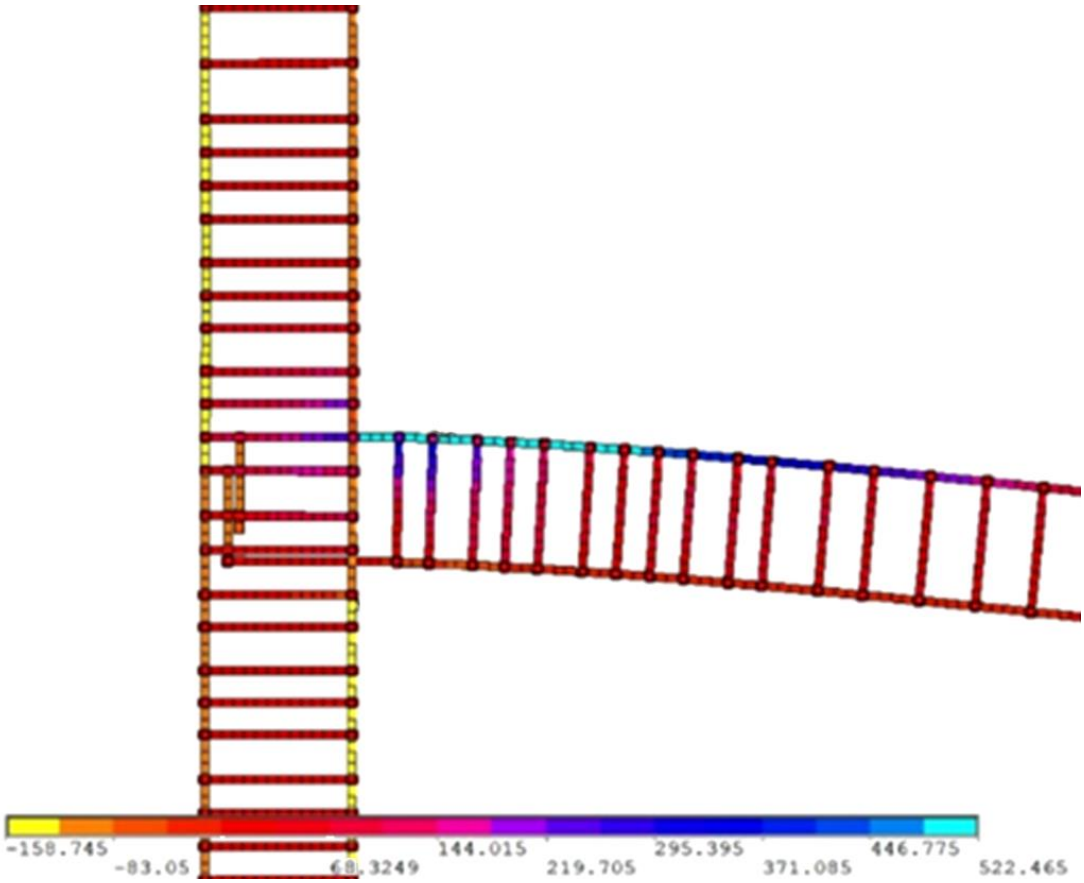

Figure 12. Steel reinforcement stress under critical load combination.

For this load combination, an SMA plate with a uniform thickness was designed and bonded to the system as the next step for the system to stay within the safety margins under the critical load combination. An empirical equation (see Equation (1)) developed by Paulay and Priestley [88] was used to specify the plastic hinge region of the joint. The calculated length was around 300 mm.

$$L_p = 0.08 \cdot L + 0.022 \cdot D_b \cdot f_y, \quad (1)$$

The plate was accordingly assigned an initial uniform thickness of 15 mm and a length equal to the plastic hinge region's length plus the column's width. The plate also extended towards the upper and lower columns for the same distance L_p. Then, do-while loops were employed to verify the length of the plastic hinge region, extensions, and the thickness of the plate installed at the joint under the critical load combination. The plastic hinge region's length was changed from 300 to 500 with an increment of 50 mm. Upper and lower extensions were also reduced from 300 mm to 0 mm with an interval of 50 mm. Using another do-while loop, the plate's thickness gradually decreased from 15 mm to 5 mm with an increment of 2 mm. For each loop repetition, the maximum free end displacement of the beam, the maximum axial stress of the steel bars and the maximum stress of the SMA were recorded. After the completion of all do-while repetitions and observation of the recorded results, the most optimised plate thickness was derived, as shown in Figure 13.

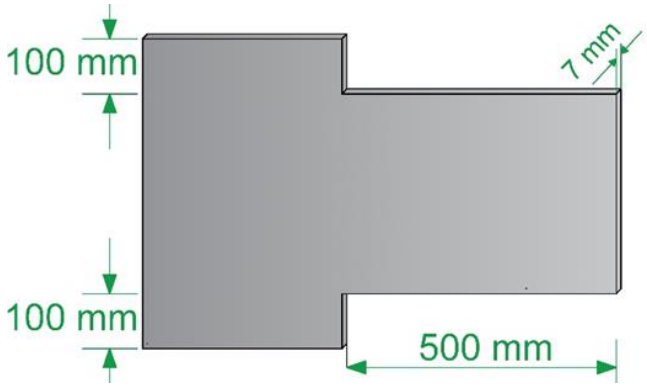

Figure 13. Initial geometry of the SMA plate designed under the critical load combination.

3.3. Optimisation of the Plate Thickness through a Probabilistic Damage Prediction

Initially, thirty-six control nodes were selected on the external surface of the SMA plate (see Figure 14). Once the initial size of the plate was calculated and the plate was simulated as installed at the joint, the same load combinations as previously were applied to the system. Load combinations were used in two different configurations: once in a cyclic form and once in a reverse cyclic form. When the cyclic load was applied, R_1 was introduced incrementally. Then, R_2 and R_3 were gradually introduced to the model. The coincident node between the internal surface of the SMA plate and the external surface of the concrete were merged to have a full connection in between; however, after the optimisation step, a contact algorithm was applied there, and a certain number of bolts were designed to fasten the plate with concrete. The main aim was to investigate the system's response when the plate was connected using a normal bolting system or a rigid interface (e.g., construction glue).

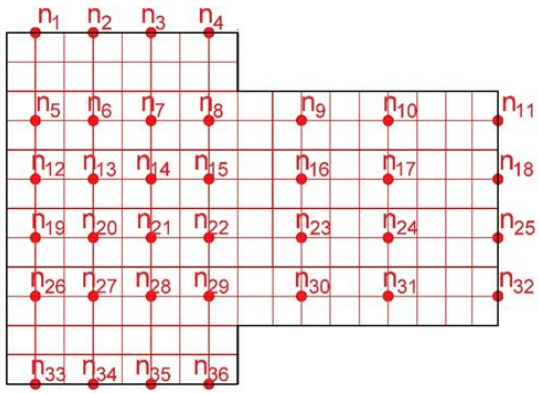

Figure 14. Schematic view of distributed control nodes over the SMA plate.

The output was then obtained in the form of the probability density functions (PDF) and cumulative distribution functions (CDF) of the stress at each control node. From the CDF diagram, the 0.95 quantile values of each control node were calculated and set as design stress. The thickness of each node was then calculated proportionately based on the associated design stress, leading to a plate with varied thicknesses but resisting failure under random cyclic loads R_1, R_2 and R_3.

The same procedure was followed to design the SMA plate for the system under reversed cyclic loads. For this case, loads were applied in four steps: (i) R_1 was applied gradually up to its maximum value; (ii) R_2 and R_3 were applied incrementally up to their maximum values; (iii) R_2 was exerted in the opposite direction, while R_1 and R_3 stayed as their maximum values; (iv) R_2 was exerted in the same direction as the second step, while R_1 and R_3 remained constant. The simulations were carried out for the new loading combination, the stress of the control nodes was recorded, and a probabilistic analysis

was performed again to design and optimise the thickness of the plate as for the cyclic actions above.

3.4. Bolting the Optimised SMA Plate to the Concrete via Fastening Technique

As a connection detailing, six bolts were assumed to fasten the optimised SMA plates to the system. The bolts were applied at those areas of the plate that had lower stress values. Beam element 188 was employed to simulate the bolts as cylindrical elements. Figure 15 demonstrates the geometry and size of the bolts. The bilinear isotropic hardening model was used to model the behaviour of the steel bolts. Figure 16 lists all the material properties of the bolts.

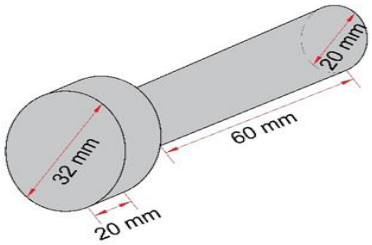

Figure 15. Geometry of the bolt.

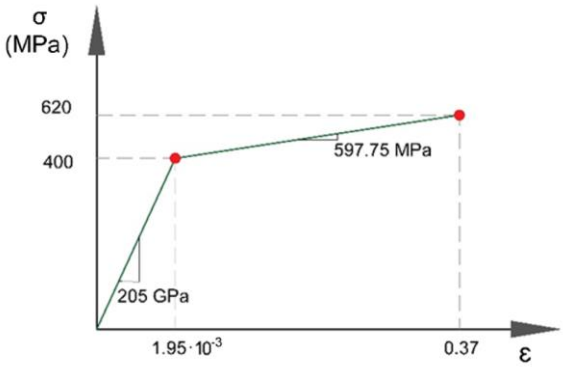

Figure 16. Material properties of the bolt.

Furthermore, a surface-to-surface contact was applied between the concrete's external surface and the plate's inner face. For this purpose, contact element 174 and target element 170 were utilised. The constitutive contact formulation observed the multipoint constraint (MPC) algorithm. The contact's function was modelled as non-separable and only sliding was possible. The MPC contact algorithm was chosen in this non-linear analysis to avoid convergence issues instead of penalty functions and Lagrange multiplier algorithms.

4. Results and Discussion

4.1. Reinforced System with SMA Plate under Cyclic Load

A probabilistic analysis for all control nodes was performed after their data were imported into MATLAB software to optimise the plate's thickness. Due to a large number of data and nodes, only the results of some significant nodes are presented herein. Diagrams of probability density functions (PDF) and cumulative distribution functions (CDF) of the node possessing maximum stress distributed over the plate are shown in Figure 17 (left and right respectively). The maximum stress appeared at the top corner of the beam–column joint. The fitted distribution type for the node was of Kernel type, which is a nonparametric distribution. This type of distribution can be employed in place of parametric distributions since it describes the results with high fitting precision. According to the associated PDF graph, the distribution's mean, standard deviation and variance were equal to 130, 40, and 129 MPa, respectively. The CDF diagram was accordingly sketched. Consequently, any quantile of the results could be calculated. Figure 17 (right) shows the CDF diagram,

where 183.79 MPa is the 95th quantile of the results. Since this node possessed maximum stress, the maximum thickness of the plate was designed accordingly, and each control node underwent this exact process.

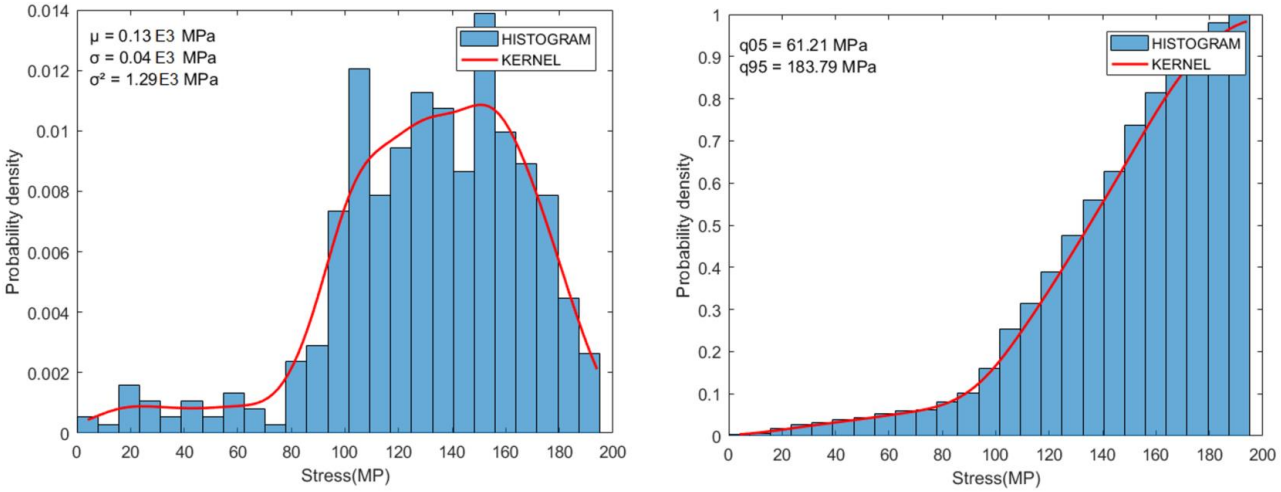

Figure 17. PDF and CDF diagrams of maximum stress node (**left** and **right** respectively).

As discussed above, due to the nature of the results, most node results were generally fitted to kernel distribution except a few; one of them is node number 27, where the generalised-extreme-value distribution was well fitting. This type is noticeably interchangeable with log-normal distribution, but since there are several negative values among the stress data, the log-normal type is excluded. PDF and CDF diagrams of this node are shown in Figure 18. It is evident that the imposed stresses and mean value are marginal since the node is located in the lower half of the plate close to the bottom surface of the beam, where the section acts mainly under compression. Figure 19 shows the SMA plate with varying thicknesses that was designed as a result of the probabilistic study.

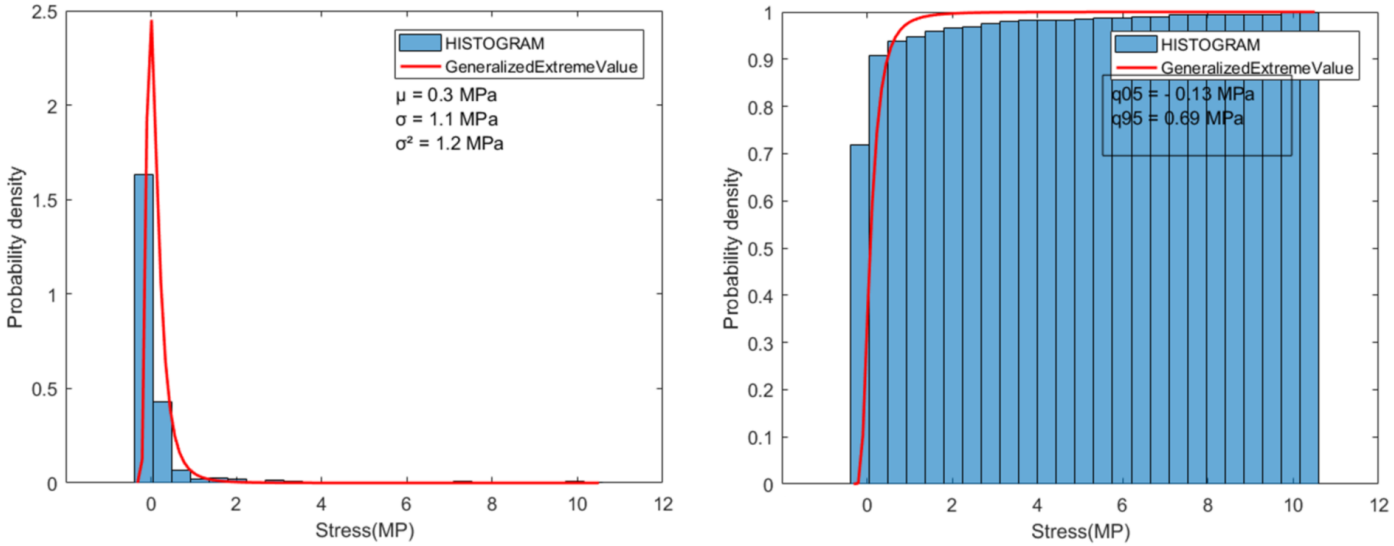

Figure 18. PDF and CDF diagrams of node number 27 (**left** and **right** respectively).

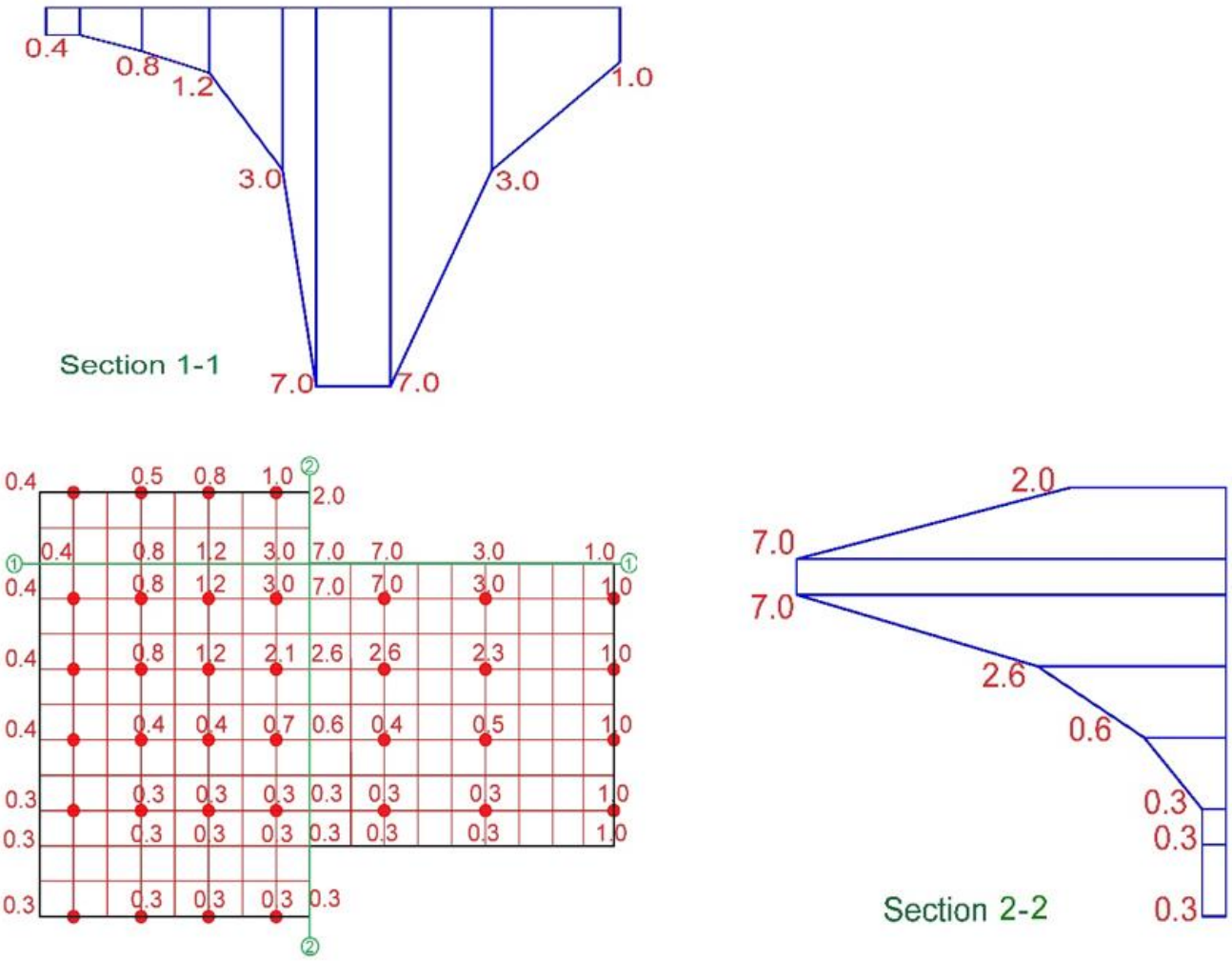

Figure 19. Optimised SMA plate based on probabilistic analysis for the system under cyclic loading (thickness is indicated with values in mm).

4.2. Reinforced System with SMA Plate under Reverse-Cyclic Load

A probabilistic study was also carried out for the control nodes of the system under a reverse cyclic loading. However, nodes 19–36 were under the same conditions as nodes 1–18 if one more load step occurred because the designed thickness of the upper half of the plate was calculated as nearly symmetrical with the lower half of the plate. The mean value and 95th quantiles of stress for the system under cyclic load were 130 and 183.79 MPa, respectively, with these values reaching 136.1 and 192.8 MPa under reverse cyclic. The PDF and CDF diagrams of the data are shown in Figure 20. In addition, the distribution type of the node that possessed maximum stress in both systems was identical (kernel distribution), and the only difference was magnitude. To optimise the plate's thickness for the system under reverse cyclic load consideration, the probabilistic study for all thirty-six control nodes was reiterated. Nonetheless, due to the large size of the dataset, only the results of the node that possessed maximum stress are presented. Figure 21 shows the SMA plate with various thicknesses designed against the results of the probabilistic study for the system under reverse cyclic loading.

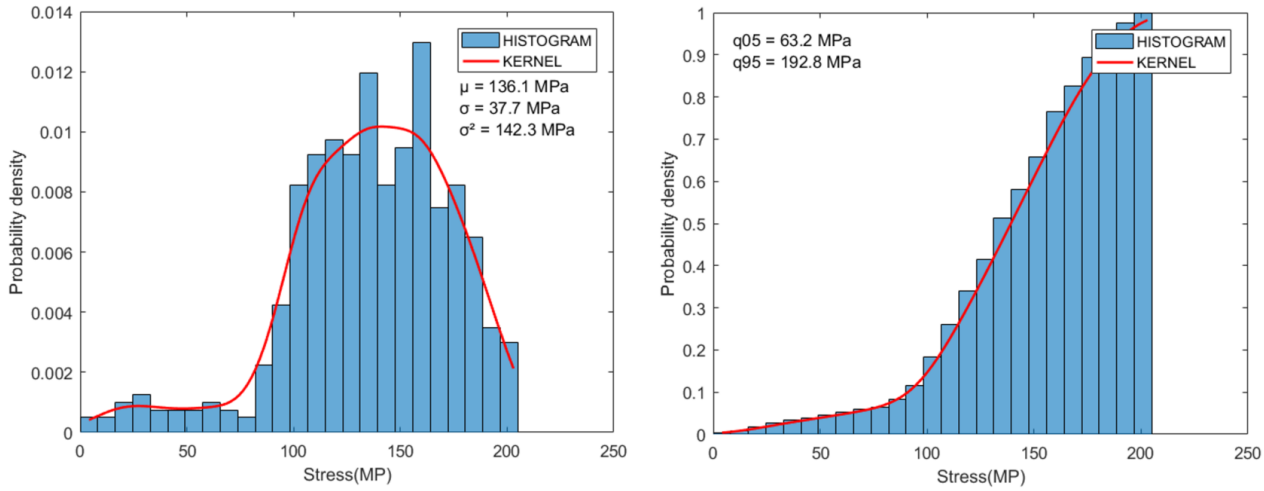

Figure 20. PDF and CDF diagrams of node number 27 (**left** and **right,** respectively).

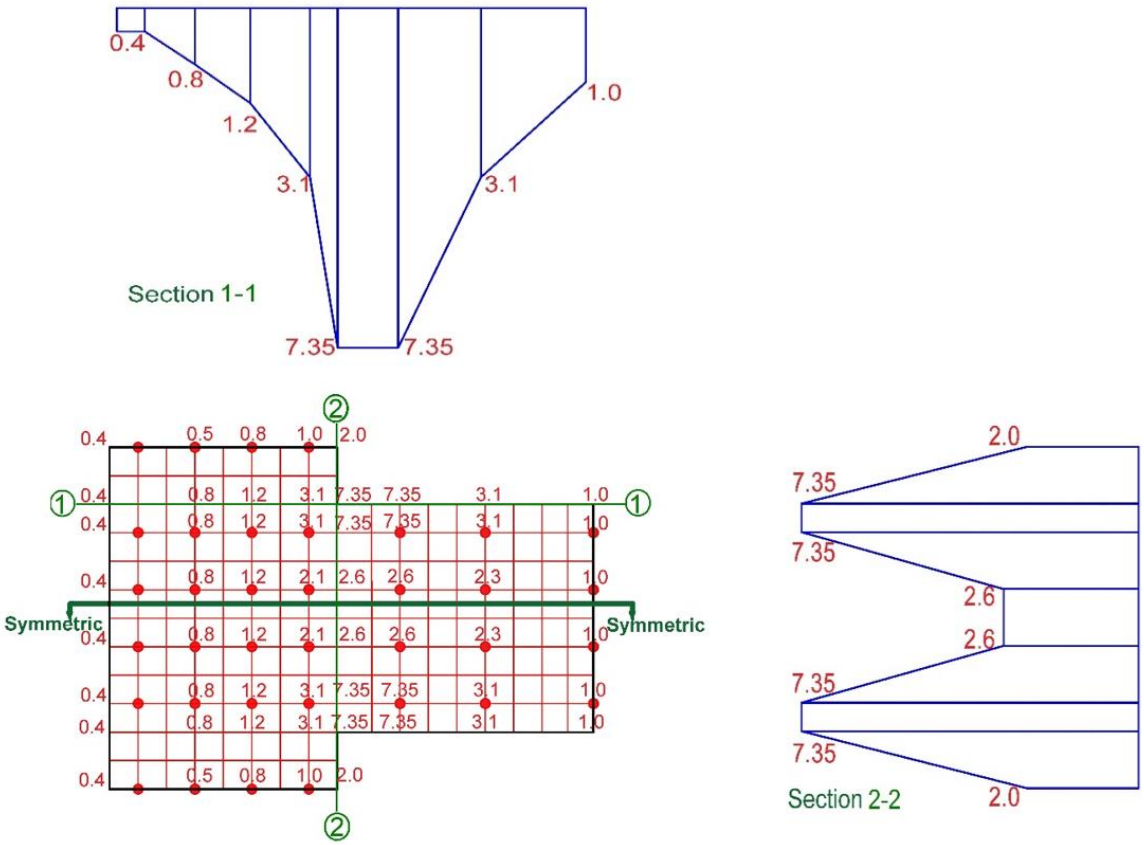

Figure 21. Optimised SMA plate for the system under reverse cyclic loading (thickness is indicated with values in mm).

4.3. Numerical Examples for System Reinforced with Optimised Plate

After this procedure, the system strengthened with the optimised SMA was finally re-examined. The system was loaded under load combinations under which the unstrengthened system failed. Two numerical checks were run: (i) the SMA strengthened joint plate under cyclic, and (ii) under reverse cyclic. In addition, each of these two examples was run twice, i.e., once before bolting the plate to the concrete joint and once after. This allowed for comparison between the plate installation and the different techniques of direct bonding and bolting. To create a rigid connection between the plate and concrete in the

model, coincident nodes at the interface were merged for examples without bolts. In the first example, the system reinforced with the optimised SMA plate bolted to the joint was loaded under cyclic loading, where R_1 had the same value as the experimental investigation, 350 kN. At the same time, R_2 was applied under displacement control up to −32 mm. The system without the SMA plate under the loading mentioned above was also considered a reference for comparison purposes. The load–displacement behaviour of both methods is shown in Figure 22. The steel bars started yielding in the reference system at a bending load (R_2) equal to 58.8 kN, but the value was 1.4 times greater in the system reinforced with the optimised SMA plate. The load-bearing capacity of the reinforced system in the elastic regime was higher than the unreinforced structure. The capability in the plastic regime was even higher so that the load-carrying capacity of the reinforced system at the displacement of 32 mm was approximately 98 kN. However, the value was only around 66 kN in the system without the plate, meaning that the existence of the plate for higher load values was a significant contribution in comparison with the system under smaller pressure. Another important finding is that the bar yielding occurred precisely at the beam–column intersection in the case without the plate. In contrast, this yielding location in the case of the strengthened joint was shifted toward the beam span beyond the plate length's end. In such a case, any failure will lead to severe damage to the beam, not the joint. Therefore, not only can the plate delay the local failure of the structure, but it can also mitigate the failure of the entire structure in case a joint capacity design is required for robustness purposes.

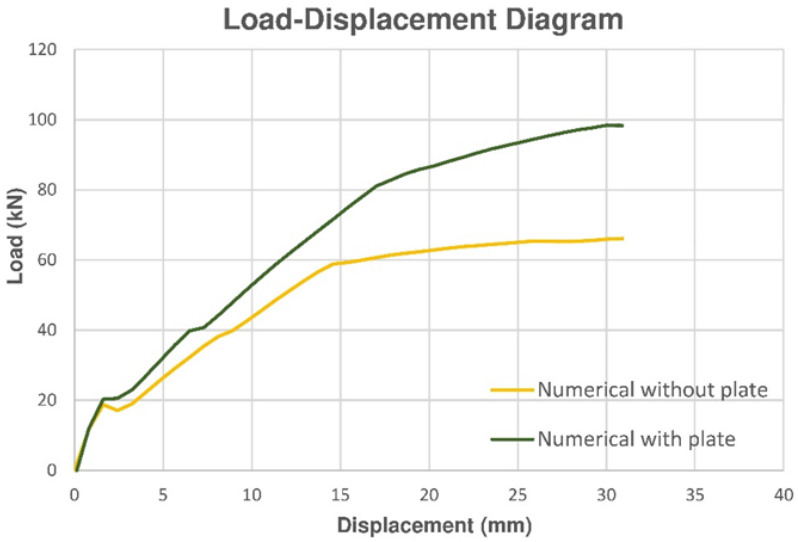

Figure 22. Load–displacement behaviour of the system with and without SMA plate under cyclic load.

The second numerical trial was done for the system strengthened with the optimised SMA plate bolted to the joint under reverse cyclic loading of load combination 192, where R_2 possessed 95% of all R_2 values. The load values of R_1, R_2 and R_3 of the load combination were 1751.82 kN, 77.912 kN and zero, respectively. Figure 23 shows the steel bars' stress, the system's maximum displacement, and stress distributed over the SMA plate for the numerical trials with and without the bolting technique. The maximum stress of the plate, which was 365 MPa, moved towards the location of the bolts in the system with the bolted SMA plate. In comparison, it was only 197 MPa and located around the upper beam–column intersection in the example without the bolting technique. In addition, the maximum axial stress of rebar for the system with bolts reached about 495 MPa, which was still less than the yielding stress of the main steel bars and was located far from the intersection. The value was 490 MPa in the system without the bolts. Hence, the bolting technique can be considered a proper method for fastening the plate to the concrete joint.

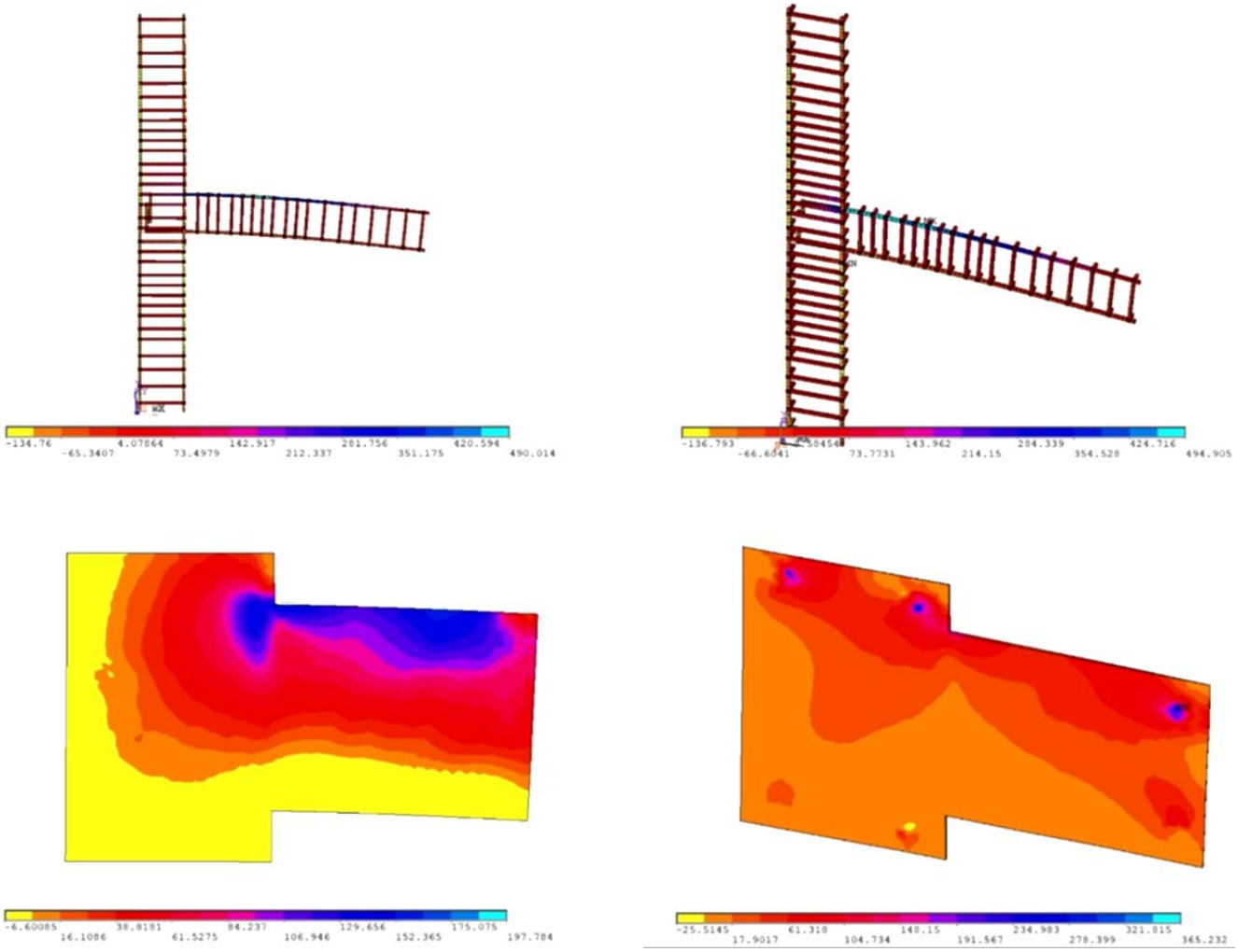

Figure 23. Results for the rebar response (**up**) and the retrofitting plate (**down**) with an assumed rigid interface such as full bond by construction glue (**left**) and with bolted assemblage (**right**).

5. Design Recommendation

Although the bolting technique shows an efficient way to fix the SMA plate to the concrete joint, the increase in the maximum stress value and the movement of its concentricity around the bolts can be considered a weak installation and, consequently, early failure of the fastening. Figure 24 demonstrates this drawback of the fastening technique and behaviour of the optimised SMA plate bolted to the joint under reverse cyclic loading in different load steps. Therefore, a locally thickened SMA plate around the bolts is needed to reduce the value and concentricity of stress around them to overcome this bolting connection disadvantage. Alternatively, bonding the plate to the joint is recommended. Regarding bolting, a design of the bolts according to current standards on fastenings (e.g., EN 1992-4 [89] in Europe) and by the use of anchor bolt products certified for seismic cyclic loads (e.g., according to the respective European Assessment Document [90]) is envisaged. Care should be given that the anchors comply with the design situation which is subject to the designer's expertise or appropriate standards' provisions. Some experimental examples and concepts for strengthening by bolted plates are given in [91–94]. The bonded plate solution (notwithstanding that both bolting and bonding can be used redundantly) may rely on the established techniques which have also been now to some extent standardised [95,96], while several applications have already been demonstrated in research and practice [97–99]. A comparison of the two connection methods is also given in [100].

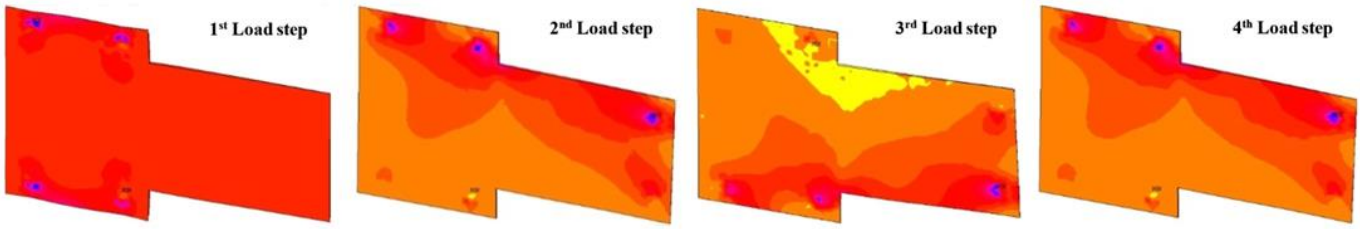

Figure 24. Stress of the SMA plate after different load steps.

Figure 25 shows an example of the recommended method of reduction of the maximum stress value around the bolts located in section D-D of the plate optimised for the system under reverse cyclic loading. As an alternative fastening method, the employment of a bonding mortar (e.g., of epoxy-based resin or equally rigid and robust material) between the plate's internal surface and the concrete's external surface must be investigated experimentally. In such a case, the value of maximum stress over the plate will also be reduced.

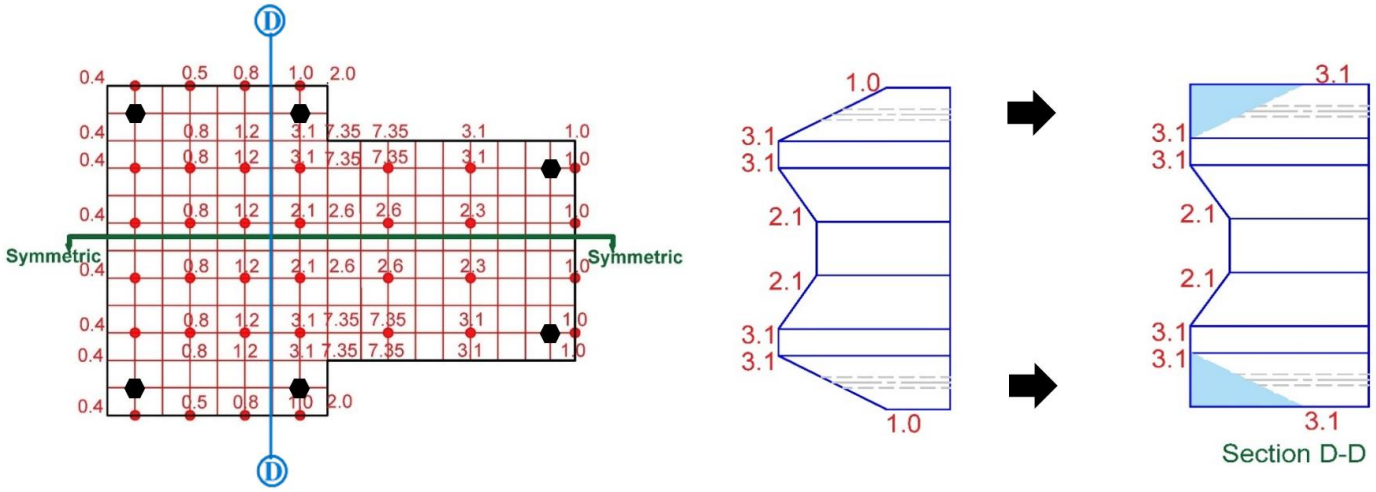

Figure 25. Design recommendation to reduce the concentricity and intensity of maximum stress around the bolts (thickness is indicated with values in mm).

6. Summary and Concluding Remarks

A numerical study has been conducted to assess the behaviour of RC beam–column joints externally bonded with an SMA plate, which was also optimised through a probabilistic damage prediction. An experimentally investigated concrete beam–column joint was simulated in Ansys software and loaded under three load types, namely axial column load (R1), bending load (R2) and axial load applied at the free end beam (R3). After mesh size convergence, verification and validation, the numerical results showed good compatibility with the experimental results in terms of load–displacement behaviour and load value leading to the yielding of the steel bars. There the point of rebar yielding was detected, corresponding to a bending load of 58 kN at a displacement of 15 mm, and a bending load of limit state functions for the system under loads R1, R2 and R3 were estimated, and the system was loaded under 1000 load combinations selected randomly from the limit state functions. The critical load combination was found, in which R1, R2 and R3 were equal to 2100.2 kN, 82.8 kN and 0 kN, respectively. The load combination led to a free end displacement of 26.25 mm and axial stress of rebar 522.5 MPa. The initial geometry of the SMA plate was designed under critical load combination using an empirical equation and some do-while loops. The designed plate had a 500 mm length, a 7 mm uniform thickness and a 100 mm extension toward the upper and lower columns. Optimisation of the plate's thickness based on the result of a probabilistic study was carried out, in

which various strengthening and loading configurations were investigated. The Kernel distribution was the overall best-fit distribution for the probabilistic results, and the 95th quantiles were considered the design stress. Two plates have been optimised, one for cyclic with a maximum thickness of 7 mm and another for a reverse cyclic loading system with a maximum thickness 7.35 mm. The plates have been assumed either bonded or bolted to the concrete beam–column joints. Some numerical examples were carried out to compare the numerical results with the experimental results and to check whether the designed plate and bolting technique worked adequately.

Furthermore, a design recommendation is proposed to reduce the stress concentration around the bolts by introducing a local thickening, which may also form a requirement for practical assembly. Replacement of the bolting fastening technique by bonding (e.g., through various upcoming construction glue technologies) can offer an alternative for even simpler and more rapid applications. In addition, the system reinforced with an externally bonded and optimised SMA plate showed significant improvement in terms of yielding and total displacement in comparison with the system without the plate, so that the rebar started yielding under bending load 81.2 kN as opposed to 58.8 kN in the system without the plate. Furthermore, the maximum axial stress of the steel bars moved towards the middle of the beam in the system with the plate, by which the risk of failure of the entire structure could be reduced and changed to failure of the beams only.

The numerical analyses presented herein demonstrate the feasibility and benefits of such a strengthening method with the advanced SMA as construction material, which form a main objective of this study. As future work, an experimental investigation under the same conditions as the numerical examples can be carried out for validation of the numerical results. In this case, both the bolted and bonded alternatives need to be tested, with particular focus, moreover, on the influences of installation quality. Such strengthening tests are recommended to be carried out, taking account of the pre-damaged situation of the concrete element, which is a realistic condition. A parametric study in which material properties of concrete and the constitutive law of the alloy are set as the main design variables can allow further exploration of suitable material properties and plate configurations.

Nonetheless, basic steps have already been taken. Based on this research, it has been made possible to understand the behaviour of the proposed strengthening system for the first time in the scientific and technical literature. The authors can only pronounce here the significance of maintaining the fact that such methods need to be rapid, minimally invasive and cost-efficient in order to adequately address the crisis following a disaster. Apart from that, the engineering community should rely on these aspects in order to improve the incentives and motivations of building owners towards structural rehabilitation measures. Additionally, a novel design approach which accounts for high uncertainties in load actions and the pre-damaged state of the concrete structures, namely probabilistic damage modelling, is demonstrated herein. Relying on this methodology, it is possible to develop optimised dimensioning of SMA structural components, which is suitable for a broad envelope of design situations. Finally, the serial industrial production of such components should be pursued so that upscaling allows a reduction in material and application costs.

Supplementary Materials: The following supporting information can be downloaded at: https://www.mdpi.com/article/10.3390/su15043831/s1. Additional information on the finite element model formulations and input proper-ties, a table of symbols and notations, as well as a flowchart of the prepared algorithms can be found in the "Supplementary Materials" file.

Author Contributions: Conceptualisation, P.S. and F.-J.B.; methodology, P.S.; software, F.-J.B.; validation, M.A.M. and P.S.; formal analysis, M.A.M.; investigation, M.A.M.; resources, F.-J.B.; data curation, M.A.M.; writing—original draft preparation, M.A.M. and P.S.; writing—review and editing, P.S.; visualisation, M.A.M.; supervision, P.S. and F.-J.B.; project administration, F.-J.B.; funding acquisition, M.A.M. and F.-J.B. All authors have read and agreed to the published version of the manuscript.

Funding: This research received no external funding. The research stay of M.A.M. in Germany was funded by the German Academic Exchange Service (Deutscher Akademischer Austauschdiens DAAD) under the programme "Research Grants—Doctoral Programmes in Germany".

Institutional Review Board Statement: Not applicable.

Informed Consent Statement: Not applicable.

Data Availability Statement: Not applicable.

Conflicts of Interest: The authors declare no conflict of interest.

References

1. Naddaf, M. Turkey-Syria earthquake: What scientists know. *Nature* **2023**, *614*, 398–399. [CrossRef]
2. Deutsche Welle. Turkey-Syria Quakes: 'Worst Natural Disaster' in a Century. 2023. Available online: https://www.dw.com/en/turkey-syria-earthquakes-worst-natural-disaster-in-a-century/a-64696911 (accessed on 14 February 2023).
3. Verisk Analytics Inc. Verisk Estimates Economic Losses from February 6 Earthquakes in Turkey Likely to Exceed USD 20 Billion. 2023. Available online: https://www.verisk.com/newsroom/verisk-estimates-economic-losses-from-february-6-earthquakes-in-turkey--likely-to-exceed-usd-20-billion/ (accessed on 14 February 2023).
4. Hojdys, Ł.; Krajewski, P.; Kwiecień, A.; Rousakis, T.; Vanian, V.; Tekieli, M.; Viskovic, A.; Ilki, A.; Gams, M.; Rakicevic, Z.; et al. Quick Repair of Damaged Infill Walls with Externally Bonded FRPU Composites: Shake Table Tests. *J. Compos. Constr.* **2023**, *27*, 04022084. [CrossRef]
5. Triantafyllou, G.G.; Rousakis, T.C.; Karabinis, A.I. Axially loaded reinforced concrete columns with a square section partially confined by light GFRP straps. *J. Compos. Constr.* **2015**, *19*, 04014035. [CrossRef]
6. Kunz, J. Missing Links: Solutions to Add Reinforcement in Existing Concrete. In Proceedings of the 2nd International Workshop on Advanced Materials and Innovative Systems in Structural Engineering: Novel Researches, Istanbul, Turkey, 20 September 2019; pp. 25–40.
7. Chellapandian, M.; Prakash, S.S.; Sharma, A. Axial compression–bending interaction behavior of severely damaged RC columns rapid repaired and strengthened using hybrid FRP composites. *Constr. Build. Mater.* **2019**, *195*, 390–404. [CrossRef]
8. Sasmal, S.; Nath, D. Evaluation of performance of non-invasive upgrade strategy for beam–column sub-assemblages of poorly designed structures under seismic type loading. *Earthq. Eng. Struct. Dyn.* **2016**, *45*, 1817–1835. [CrossRef]
9. Kanchanadevi, A.; Ramanjaneyulu, K. Non-invasive hybrid retrofit for seismic damage mitigation of gravity load designed exterior beam–column sub-assemblage. *J. Earthq. Eng.* **2021**, *25*, 1590–1615. [CrossRef]
10. fib Task Group 8.1. *fib Bulletin 103—Guide for Strengthening of Concrete Structures*; fib—The International Federation for Structural Concrete: Lausanne, Switzerland, 2022.
11. Van Breugel, K. Is there a market for self-healing cement-based materials. In Proceedings of the 1st International Conference on Self-Healing Materials, Noordwijk, The Netherlands, 18–20 April 2007.
12. Abdulrahman, A.; Ismail, M.; Hussain, M.S. Corrosion inhibitors for steel reinforcement in concrete: A review. *Sci. Res. Essays* **2011**, *6*, 4152–4162. [CrossRef]
13. Shanmugam, S.; Srisanthi, V.; Ramachandran, S. Effects of Corrosion on Reinforced Concrete Beams with Silica Fume and Polypropylene Fibre. *Int. J. Civ. Environ. Struct. Constr. Archit. Eng.* **2013**, *7*, 151–156.
14. Fardis, M.N. Shear strength model for RC joints, consistent with the shear design rules for prismatic members in the second-generation Eurocodes. *Bull. Earthq. Eng.* **2021**, *19*, 889–917. [CrossRef]
15. Nasrollahzadeh, K.; Hariri-Ardebili, M.A.; Kiani, H.; Mahdavi, G. An Integrated Sensitivity and Uncertainty Quantification of Fragility Functions in RC Frames. *Sustainability* **2022**, *14*, 13082. [CrossRef]
16. Fascetti, A.; Kunnath, S.K.; Nisticò, N. Robustness evaluation of RC frame buildings to progressive collapse. *Eng. Struct.* **2015**, *86*, 242–249. [CrossRef]
17. Praxedes, C.; Yuan, X.X. Robustness-oriented optimal design for reinforced concrete frames considering the large uncertainty of progressive collapse threats. *Struct. Saf.* **2022**, *94*, 102139. [CrossRef]
18. Spyridis, P.; Strauss, A. Robustness assessment of redundant structural systems based on design provisions and probabilistic damage analyses. *Buildings* **2020**, *10*, 213. [CrossRef]
19. Strauss, A.; Pürgstaller, A.; Pampanin, S.; Spyridis, P.; Bergmeister, K. Robustheit von Ingenieurstrukturen. In *BetonKalender 2022: Nachhaltigkeit, Digitalisierung, Instandhaltung*; Wilhelm Ernst & Sohn: Berlin, Germany, 2022; pp. 375–420.
20. Li, V.C.; Herbert, E. Robust self-healing concrete for sustainable infrastructure. *J. Adv. Concr. Technol.* **2012**, *10*, 207–218. [CrossRef]
21. Bostenaru Dan, M. Decision making based on benefit-costs analysis: Costs of preventive retrofit versus costs of repair after earthquake hazards. *Sustainability* **2018**, *10*, 1537. [CrossRef]
22. Tsonos, A.D.; Kalogeropoulos, G. Analytical model for the design of HSFC and UHSFC Jackets with various steel fiber volume fraction ratios for the retrofitting of RC beam-column joints. *Sustainability* **2021**, *13*, 11209. [CrossRef]
23. Tsonos, A.D.G. Performance enhancement of R/C building columns and beam–column joints through shotcrete jacketing. *Eng. Struct.* **2010**, *32*, 726–740.

24. Araby, M.Z.; Rizal, S.; Afifuddin, M.; Hasan, M. Deformation Capacity of RC Beam-Column Joints Strengthened with Ferrocement. *Sustainability* **2022**, *14*, 4398. [CrossRef]
25. Beschi, C.; Meda, A.; Riva, P. Column and joint retrofitting with high performance fiber reinforced concrete jacketing. *J. Earthq. Eng.* **2011**, *15*, 989–1014. [CrossRef]
26. Santarsiero, G.; Masi, A. Seismic performance of RC beam–column joints retrofitted with steel dissipation jackets. *Eng. Struct.* **2015**, *85*, 95–106.
27. Shafaei, J.; Hosseini, A.; Marefat, M.S. Seismic retrofit of external RC beam–column joints by joint enlargement using prestressed steel angles. *Eng. Struct.* **2014**, *81*, 265–288. [CrossRef]
28. Golias, E.; Zapris, A.G.; Kytinou, V.K.; Kalogeropoulos, G.I.; Chalioris, C.E.; Karayannis, C.G. Effectiveness of the novel rehabilitation method of seismically damaged RC joints using C-FRP ropes and comparison with widely applied method using C-FRP sheets—Experimental investigation. *Sustainability* **2021**, *13*, 6454. [CrossRef]
29. Ghobarah, A.; Said, A. Seismic rehabilitation of beam-column joints using FRP laminates. *J. Earthq. Eng.* **2001**, *5*, 113–129. [CrossRef]
30. Karabinis, A.I.; Rousakis, T.C. Seismic rehabilitation of reinforced concrete beam-column connections by FRP material. In Proceedings of the International Conference on Computational & Experimental Engineering & Sciences ICCES, Modeira, Portugal, 26–29 July 2004; Volume 4, pp. 26–29.
31. Akguzel, U.; Pampanin, S. Assessment and design procedure for the seismic retrofit of reinforced concrete beam-column joints using FRP composite materials. *J. Compos. Constr.* **2012**, *16*, 21–34. [CrossRef]
32. Pohoryles, D.A.; Melo, J.; Rossetto, T.; Varum, H.; Bisby, L. Seismic retrofit schemes with FRP for deficient RC beam-column joints: State-of-the-art review. *J. Compos. Constr.* **2019**, *23*, 03119001. [CrossRef]
33. DesRoches, R.; McCormick, J.; Delemont, M. Cyclic properties of superelastic shape memory alloy wires and bars. *J. Struct. Eng.* **2004**, *130*, 38–46. [CrossRef]
34. Zhou, X.; Ke, K.; Yam, M.C.; Zhao, Q.; Huang, Y.; Di, J. Shape memory alloy plates: Cyclic tension-release performance, seismic applications in beam-to-column connections and a structural seismic demand perspective. *Thin-Walled Struct.* **2021**, *167*, 108158. [CrossRef]
35. Janke, L.; Czaderski, C.; Motavalli, M.; Ruth, J. Applications of shape memory alloys in civil engineering structures—Overview, limits and new ideas. *Mater. Struct.* **2005**, *38*, 578–592.
36. Cladera, A.; Weber, B.; Leinenbach, C.; Czaderski, C.; Shahverdi, M.; Motavalli, M. Iron-based shape memory alloys for civil engineering structures: An overview. *Constr. Build. Mater.* **2014**, *63*, 281–293. [CrossRef]
37. Shahverdi, M.; Michels, J.; Czaderski, C.; Motavalli, M. Iron-based shape memory alloy strips for strengthening RC members: Material behavior and characterization. *Constr. Build. Mater.* **2018**, *173*, 586–599. [CrossRef]
38. Fang, C.; Qiu, C.; Zheng, Y. Shape Memory Alloys for Civil Engineering. *Materials* **2023**, *16*, 787. [CrossRef] [PubMed]
39. Zareie, S.; Issa, A.S.; Seethaler, R.J.; Zabihollah, A. Recent advances in the applications of shape memory alloys in civil infrastructures: A review. *Structures* **2020**, *27*, 1535–1550. [CrossRef]
40. Raza, S.; Shafei, B.; Saiidi, M.S.; Motavalli, M.; Shahverdi, M. Shape memory alloy reinforcement for strengthening and self-centering of concrete structures—State of the art. *Constr. Build. Mater.* **2022**, *324*, 126628. [CrossRef]
41. Abavisani, I.; Rezaifar, O.; Kheyroddin, A. Multifunctional Properties of Shape Memory Materials in Civil Engineering Applications: A State-of-the-Art Review. *J. Build. Eng.* **2021**, *44*, 102657. [CrossRef]
42. Leon, R.T.; DesRoches, R.; Ocel, J.; Hess, G. Innovative beam column connections using shape memory alloys. In Proceedings of the SPIE's 8th Annual International Symposium on Smart Structures and Materials, Newport Beach, CA, USA, 4–8 March 2001; Volume 4330, pp. 227–238.
43. Wang, W.; Chan, T.M.; Shao, H. Seismic performance of beam–column joints with SMA tendons strengthened by steel angles. *J. Constr. Steel Res.* **2015**, *109*, 61–71. [CrossRef]
44. Fang, C.; Zhou, X.; Osofero, A.I.; Shu, Z.; Corradi, M. Superelastic SMA Belleville washers for seismic resisting applications: Experimental study and modelling strategy. *Smart Mater. Struct.* **2016**, *25*, 105013. [CrossRef]
45. Farmani, M.A.; Ghassemieh, M. Steel beam-to-column connections equipped with SMA tendons and energy dissipating devices including shear tabs or web hourglass pins. *J. Constr. Steel Res.* **2017**, *135*, 30–48. [CrossRef]
46. Molod, M.A.; Spyridis, P.; Barthold, F.J. Applications of shape memory alloys in structural engineering with a focus on concrete construction—A comprehensive review. *Constr. Build. Mater.* **2022**, *337*, 127565. [CrossRef]
47. Varela, S. A bridge column with superelastic NiTi SMA and replaceable rubber hinge for earthquake damage mitigation. *Smart Mater. Struct.* **2016**, *25*, 075012. [CrossRef]
48. Wang, B.; Zhu, S. Seismic behaviour of self-centering reinforced concrete wall enabled by superelastic shape memory alloy bars. *Bull. Earthq. Eng.* **2018**, *16*, 479–502. [CrossRef]
49. Abraik, E.; Youssef, M.A.; El-Fitiany, S.F. Seismic Performance of Hybrid Corrosion-Free Self-Centering Concrete Shear Walls. *Sustainability* **2022**, *14*, 712. [CrossRef]
50. Michels, J.; Shahverdi, M.; Czaderski, C.; Schranz, B.; Motavalli, M. Iron based shape memory alloy strips, part 2: Flexural strengthening of RC beams. In Proceedings of the 4th International Conference on Smart Monitoring, Assessment and Rehabilitation of Civil Structures (SMAR 2017), Zurich, Switzerland, 13–15 September 2017.

51. Jung, D.; Zafar, A.; Andrawes, B. Sustainability of civil infrastructure using shape memory technology. *Innov. Infrastruct. Solut.* **2017**, *2*, 28. [CrossRef]
52. Mas, B.; Biggs, D.; Vieito, I.; Cladera, A.; Shaw, J.; Martínez-Abella, F. Superelastic shape memory alloy cables for reinforced concrete applications. *Constr. Build. Mater.* **2017**, *148*, 307–320. [CrossRef]
53. Strieder, E.; Aigner, C.; Petautschnig, G.; Horn, S.; Marcon, M.; Schwenn, M.; Zeman, O.; Castillo, P.; Wan-Wendner, R.; Bergmeister, K. Strengthening of reinforced concrete beams with externally mounted sequentially activated iron-based shape memory alloys. *Materials* **2019**, *12*, 345. [CrossRef] [PubMed]
54. Schranz, B. Iron-based Shape Memory Alloy Reinforcement for Prestressed Strengthening of Concrete Structures. Ph.D. Dissertation, ETH Zurich, Zurich, Switzerland, 2021.
55. Suhail, R.; Amato, G.; Chen, J.-F.; McCrum, D. Potential Applications of Shape Memory Alloys in Seismic Retrofitting of An Exterior Reinforced Concrete Beam-Column Joint. In Proceedings of the SECED 2015 Conference: Earthquake Risk and Engineering towards a Resilient World, Cambridge, UK, 9–10 July 2015.
56. Yurdakul, Ö.; Tunaboyu, O.; Avşar, Ö. Retrofit of non-seismically designed beam-column joints by post-tensioned superelastic shape memory alloy bars. *Bull. Earthq. Eng.* **2018**, *16*, 5279–5307. [CrossRef]
57. Elbahy, Y.; Youssef, M.; Meshaly, M. Seismic performance of reinforced concrete frames retrofitted using external superelastic shape memory alloy bars. *Bull. Earthq. Eng.* **2019**, *17*, 781–802. [CrossRef]
58. Elbahy, Y.I.; Youssef, M.A.; Meshaly, M. Numerical investigation of reinforced-concrete beam-column joints retrofitted using external superelastic shape memory alloy bars. *AIMS Mater. Sci.* **2021**, *8*, 716–738. [CrossRef]
59. Youssef, M.; Meshaly, M.; Elansary, A. Ductile corrosion-free self-centering concrete elements. *Eng. Struct.* **2019**, *184*, 52–60. [CrossRef]
60. Youssef, M.; Alam, M.; Nehdi, M. Experimental investigation on the seismic behaviour of beam-column joints reinforced with superelastic shape memory alloys. *J. Earthq. Eng.* **2008**, *12*, 1205–1222. [CrossRef]
61. Alam, M.; Youssef, M.; Nehdi, M. Analytical prediction of the seismic behaviour of superelastic shape memory alloy reinforced concrete elements. *Eng. Struct.* **2008**, *30*, 3399–3411. [CrossRef]
62. Hojatirad, A.; Naderpour, H. Seismic assessment of RC structures having shape memory alloys rebar and strengthened using CFRP sheets in terms of fragility curves. *Bull. Earthq. Eng.* **2021**, *19*, 5087–5112. [CrossRef]
63. Nahar, M.; Islam, K.; Billah, A.M. Seismic collapse safety assessment of concrete beam-column joints reinforced with different types of shape memory alloy rebars. *J. Build. Eng.* **2020**, *29*, 101106. [CrossRef]
64. Abraik, E. Seismic performance of shape memory alloy reinforced concrete moment frames under sequential seismic hazard. *Structures* **2020**, *26*, 311–326. [CrossRef]
65. Zafar, A.; Andrawes, B. Incremental dynamic analysis of concrete moment resisting frames reinforced with shape memory composite bars. *Smart Mater. Struct.* **2012**, *21*, 025013. [CrossRef]
66. Molod, M.A.M. Strengthening Reinforced Concrete Column-Beam Joints with Modular Shape Memory Alloy Plate Optimized through Probabilistic Damage Prediction. Ph.D. Dissertation, TU Dortmund, Dortmund, Germany, 2021. Available online: https://eldorado.tu-dortmund.de/handle/2003/40159 (accessed on 14 February 2023).
67. Chang, L.C.; Read, T.A. Plastic deformation and diffusionless phase changes in metals—The gold-cadmium beta phase. *JOM* **1951**, *3*, 47–52. [CrossRef]
68. Miyazaki, S.; Duerig, T.; Melton, K. *Engineering Aspects of Shape Memory Alloys*; Butterworth-Heinemann: London, UK, 1990.
69. Nasradeen, D. Self-Repairing Performance of Concrete Beams Reinforced with SMA 734 Wires. Master's Thesis, Newcastle University, Newcastle, UK, 2015.
70. Deng, Z.; Li, Q.; Sun, H. Behaviour of concrete beam with embedded shape memory alloy wires. *Eng. Struct.* **2006**, *28*, 1691–1697. [CrossRef]
71. ANSYS. *ANSYS Documentation Ansys®ANSYS Mechanical APDL, 2019.1, Help System, Ansys Documentation*; ANSYS, Inc.: Canonsburg, PA, USA, 2019.
72. *EN 1992.1-1*; Eurocode 2: Design of Concrete Structures—Part 1-1: General Rules and Rules for Buildings. European Committee for Standardization (CEN): Brussels, Belgium, 2004.
73. Shukri, A.A.; Jumaat, M.Z. The tension-stiffening contribution of NSM CFRP to the behaviour of strengthened RC beams. *Materials* **2015**, *8*, 4131–4146. [CrossRef]
74. *CSA A23.3-04*; Design of Concrete Structures. Canadian Standards Association: Mississauga, ON, Canada, 2004.
75. Bažant, Z.P.; Gambarova, P.G. Crack shear in concrete: Crack band microflane model. *J. Struct. Eng.* **1984**, *110*, 2015–2035. [CrossRef]
76. Bažant, Z.P.; Oh, B.H. Microplane model for progressive fracture of concrete and rock. *J. Eng. Mech.* **1985**, *111*, 559–582. [CrossRef]
77. Zreid, I.; Kaliske, M. Regularisation of microplane damage models using an implicit gradient enhancement. *Int. J. Solids Struct.* **2014**, *51*, 3480–3489. [CrossRef]
78. Zreid, I.; Kaliske, M. An implicit gradient formulation for microplane Drucker-Prager plasticity. *Int. J. Plast.* **2016**, *83*, 252–272. [CrossRef]
79. Zreid, I.; Kaliske, M. Microplane modeling of cyclic behaviour of concrete: A gradient plasticity-damage formulation. *PAMM* **2016**, *16*, 415–416. [CrossRef]

80. Zreid, I.; Kaliske, M. A gradient enhanced plasticity–damage microplane model for concrete. *Comput. Mech.* **2018**, *62*, 1239–1257. [CrossRef]
81. Menetrey, P. Numerical Analysis of Punching Failure in Reinforced Concrete Structures. Master's Thesis, EPFL, Lausanne, Switzerland, 1994.
82. Willam, K.J.; Warnke, E.P. Constitutive model for the triaxial behaviour of concrete. In Proceedings of the Seminar on Concrete Structure Subjected to Triaxial Stresses, Bergamo, Italy, 17–19 May 1974.
83. Rohatgi, A. WebPlotDigitizer; Austin, TX, USA. 2017. Available online: https://apps.automeris.io/wpd/ (accessed on 12 December 2022).
84. Novák, D.; Lehký, D. ANN inverse analysis based on stochastic small-sample training set simulation. *Eng. Appl. Artif. Intell.* **2006**, *19*, 731–740. [CrossRef]
85. Barkhordari, M.S.; Armaghani, D.J.; Asteris, P.G. Structural damage identification using ensemble deep convolutional neural network models. *Comput. Model. Eng. Sci.* **2022**, *134*, 835–855. [CrossRef]
86. Šomodíková, M.; Lehký, D.; Doležel, J.; Novák, D. Modeling of degradation processes in concrete: Probabilistic lifetime and load-bearing capacity assessment of existing reinforced concrete bridges. *Eng. Struct.* **2016**, *119*, 49–60. [CrossRef]
87. Strauss, A.; Frangopol, D.M.; Bergmeister, K. Assessment of existing structures based on identification. *J. Struct. Eng.* **2010**, *136*, 86–97. [CrossRef]
88. Paulay, T.; Priestley, M.J.N. *Seismic Design of Reinforced Concrete and Masonry Buildings*; John Wiley Sons, Inc.: Hoboken, NJ, USA, 1992.
89. *EN 1992–4:2018*; Eurocode 2—Design of Concrete Structures—Part 4: Design of Fastenings for Use in Concrete. European Committee for Standardization: Brussels, Belgium, 2018.
90. *EAD 330232–01-0601*; Mechanical Fasteners for Use in Concrete, Decision (EU) 2021/1789. European Organisation for Technical Assessment (EOTA): Brussels, Belgium, 2021.
91. Li, L.Z.; Lo, S.H.; Su, R.K.L. Experimental study of moderately reinforced concrete beams strengthened with bolted-side steel plates. *Adv. Struct. Eng.* **2013**, *16*, 499–516. [CrossRef]
92. Aykac, S.; Kalkan, I.; Aykac, B.; Karahan, S.; Kayar, S. Strengthening and Repair of Reinforced Concrete Beams Using External Steel Plates. *J. Struct. Eng.* **2013**, *139*, 929–939. [CrossRef]
93. Liu, X.; Lu, Z.D.; Li, L.Z. The use of bolted side plates for shear strengthening of RC beams: A review. *Sustainability* **2018**, *10*, 4658. [CrossRef]
94. Marchisella, A.; Muciaccia, G.; Sharma, A.; Eligehausen, R. Experimental investigation of 3d RC exterior joint retrofitted with fully-fastened-haunch-retrofit-solution. *Eng. Struct.* **2021**, *239*, 112206. [CrossRef]
95. *EAD 160086-00-0301*; Kits for the Strengthening of Concrete Elements by Externally Bonded CFRP Strips. European Organisation for Technical Assessment (EOTA): Brussels, Belgium, 2023; (*in press*).
96. DafStb. *DAfStb-RiLi VBgB: Richtlinie "Verstärken von Betonbauteilen mit geklebter Bewehrung"*; Deutscher Ausschuss für Stahlbeton: Berlin, Germany, 2012.
97. Bergmeister, K. Kleben im Betonbau-Theoretische Grundlagen und Bemessungsvorschläge (Bonding in structural concrete—Theoretical basics and design proposals). *Beton-und Stahlbetonbau* **2001**, *96*, 625–633. [CrossRef]
98. Altin, S.; Anil, Ö.; Kara, M.E. Improving shear capacity of existing RC beams using external bonding of steel plates. *Eng. Struct.* **2005**, *27*, 781–791. [CrossRef]
99. Barnes, R.A.; Mays, G.C. Strengthening of reinforced concrete beams in shear by the use of externally bonded steel plates: Part 2—Design guidelines. *Constr. Build. Mater.* **2006**, *20*, 403–411. [CrossRef]
100. Barnes, R.A.; Baglin, P.S.; Mays, G.C.; Subedi, N.K. External steel plate systems for the shear strengthening of reinforced concrete beams. *Eng. Struct.* **2001**, *23*, 1162–1176. [CrossRef]